#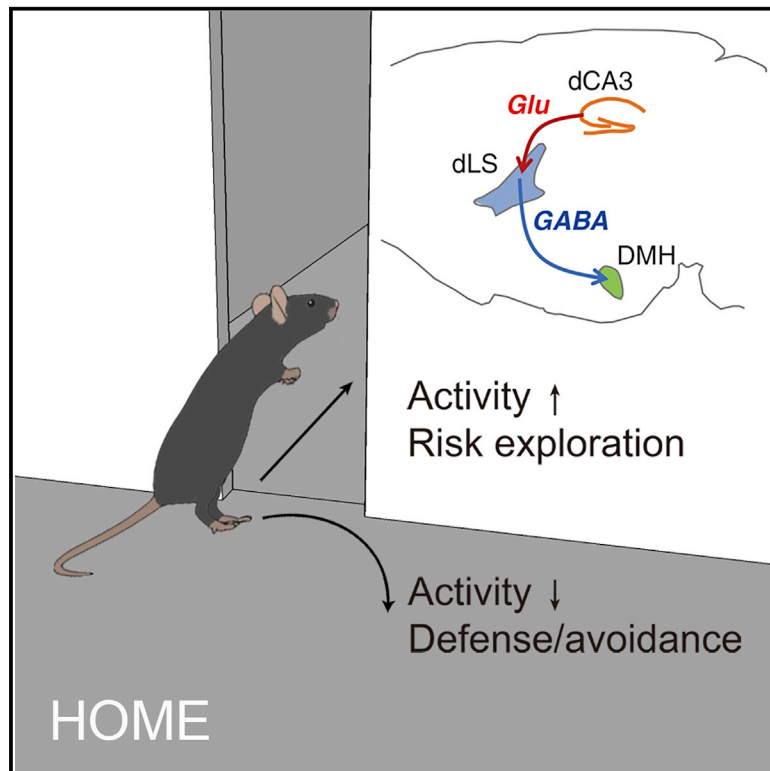 A neural circuit from the dorsal CA3 to the dorsomedial hypothalamus mediates balance between risk exploration and defense

Graphical abstract

Authors

Cheng Zhong, Lulu Wang, Yi Cao, ..., Fuqiang Xu, Yi Lu, Liping Wang

Correspondence

luyi@siat.ac.cn (Y.L.), lp.wang@siat.ac.cn (L.W.)

In brief

Zhong et al. show that dCA3[Glu] neurons respond positively to contextual exploration but negatively to potential threat. A dCA3[Glu]-dLS[GABA]-DMH circuit controlling exploration and defense balances in complex environments is identified. Activation or inhibition of this circuit bidirectionally regulates an animal's arousal level and promotes the switch between defense and risk exploration.

Highlights

- dCA3[Glu] neurons are suppressed by predatory threat and risk exploration

- A disynaptic dCA3[Glu]-dLS[GABA]-DMH circuit is identified

- This circuit controls the switch between defense and risk exploration

- Activating this circuit inhibits defense by decreasing predator-evoked arousal

CellPress

A neural circuit from the dorsal CA3 to the dorsomedial hypothalamus mediates balance between risk exploration and defense

Cheng Zhong,[1,3] Lulu Wang,[1,3] Yi Cao,[1] Chongyang Sun,[1] Jianyu Huang,[1] Xufang Wang,[1] Suwan Pan,[1] Shuyu He,[1] Kang Huang,[1] Zhonghua Lu,[1] Fuqiang Xu,[1,2] Yi Lu,[1,*] and Liping Wang[1,4,*]

[1]Guangdong Provincial Key Laboratory of Brain Connectome and Behavior, the Brain Cognition and Brain Disease Institute, Shenzhen Institute of Advanced Technology, Chinese Academy of Sciences, Shenzhen-Hong Kong Institute of Brain Science-Shenzhen Fundamental Research Institutions, Shenzhen 518055, China
[2]Center for Brain Science, Wuhan Institute of Physics and Mathematics, Center for Excellence in Brain Science and Intelligence Technology, Chinese Academy of Sciences, Wuhan 430071, China
[3]These authors contributed equally
[4]Lead contact
*Correspondence: luyi@siat.ac.cn (Y.L.), lp.wang@siat.ac.cn (L.W.)
https://doi.org/10.1016/j.celrep.2022.111570

SUMMARY

An appropriate balance between explorative and defensive behavior is essential for the survival and reproduction of prey animals in risky environments. However, the neural circuit and mechanism that allow for such a balance remains poorly understood. Here, we use a semi-naturalistic predator threat test (PTT) to observe and quantify the defense-exploration balance, especially risk exploration behavior in mice. During the PTT, the activity of the putative dorsal CA3 glutamatergic neurons (dCA3^{Glu}) is suppressed by predatory threat and risk exploration, whereas the neurons are activated during contextual exploration. Moreover, optogenetic excitation of these neurons induces a significant increase in risk exploration. A circuit, comprising the dorsal CA3, dorsal lateral septal, and dorsomedial hypothalamic (dCA3^{Glu}-dLS^{GABA}-DMH) areas, may be involved. Moreover, activation of the dCA3^{Glu}-dLS^{GABA}-DMH circuit promotes the switch from defense to risk exploration and suppresses threat-induced increase in arousal.
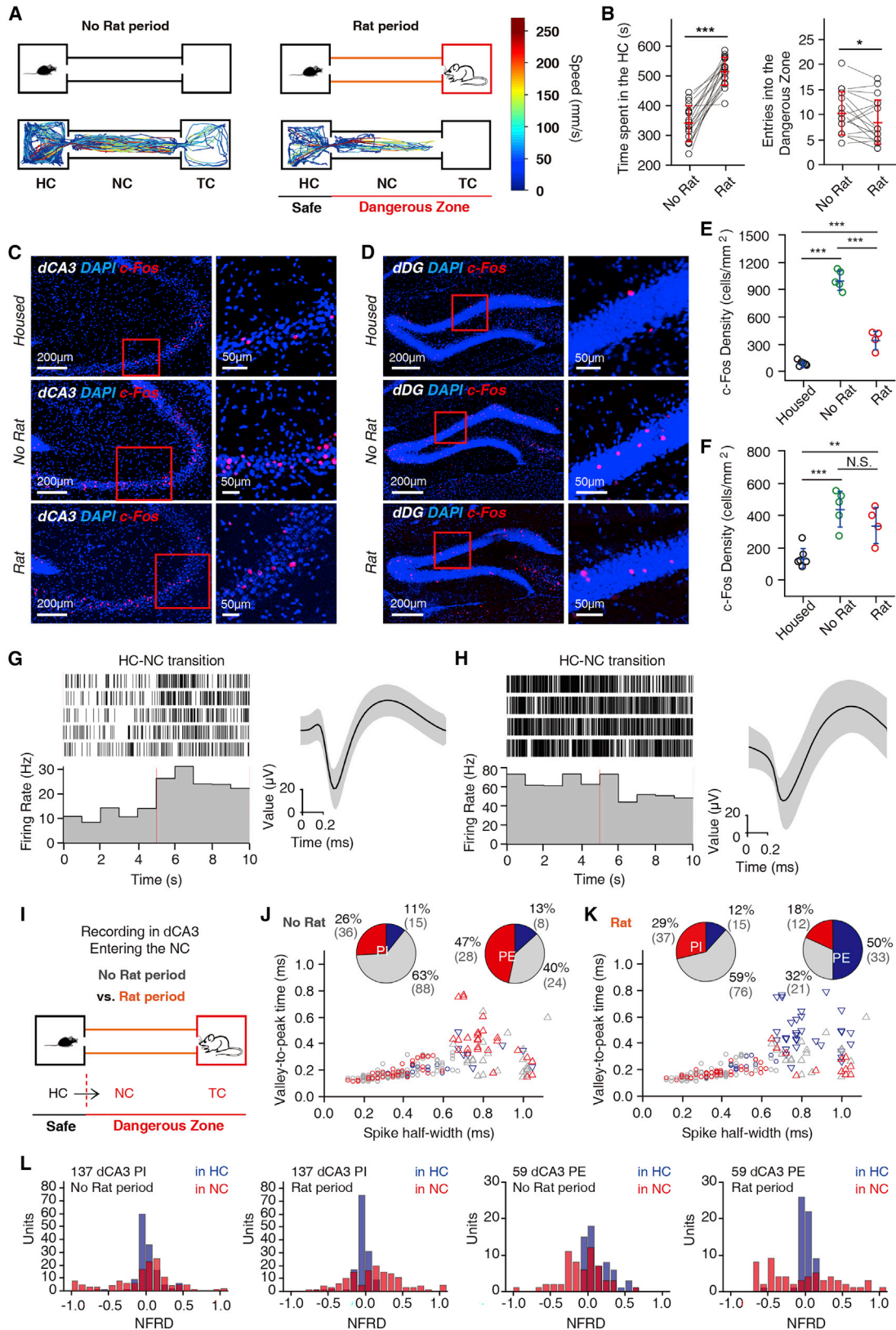
INTRODUCTION

Individual survival requires precise execution of a variety of instinctive behaviors. Because of potential threats that exist in the natural environment, for survival and reproduction, instinctive risk explorations are vital for individuals across species to attain their basic needs (food, water, mates, etc.) (Berlyne, 1966; Gottlieb and Oudeyer, 2018). Once risk information is detected during exploration, terminating exploratory behavior and initiating defensive behavior is essential for the animal to avoid potential harm from predators or other threats in the environment (Evans et al., 2019; Headley et al., 2019; LeDoux, 2012). Therefore, accurately controlling the balance between exploration and defensive behavior is crucial for prey animals to adapt to (Darwin, 1969), especially in a complex and dangerous natural environment (De La Flor et al., 2017; LeDoux, 2012; van Kampen, 2015); however, the neural circuit mechanism underlying this process remains largely unclear.

In a pre-encounter threat context, where there is a potential predator, the dorsal hippocampus (dHPC) is thought to be necessary for defensive behavior (Mobbs, 2018; Qi et al., 2018; Wikenheiser and Schoenbaum, 2016), because it is critical in environmental exploration and perception of fearful environ-

mental cues (Berger et al., 2006; Saab et al., 2009; Wang et al., 2020). Recent studies suggest that the dHPC (DG-CA3) responds to the conditioned fear paired threat context, especially ambiguous environmental threat information, specifically via the dorsal lateral septum (dLS) (Besnard et al., 2019, 2020). Moreover, the LS receives dense projections from the dHPC (Risold and Swanson, 1996; Strange et al., 2014) and subsequently modulates functions of the action-executing targets (Bender et al., 2015; Leroy et al., 2018; Luo et al., 2011; Sweeney and Yang, 2015, 2016; Tingley and Buzsaki, 2018), such as the hypothalamic structures. Therefore, the LS is considered an important relay between the dHPC and downstream regions, which translates and sends environmental information to regulate other behaviors. For instance, the dorsal CA1-dLS-lateral hypothalamic circuit modulates motion (Bender et al., 2015) and feeding behaviors (Sweeney and Yang, 2015, 2016), whereas the dorsal CA2-LS circuit projects to the ventrolateral part of the ventromedial hypothalamus to regulate aggressive behaviors (Leroy et al., 2018; Wong et al., 2016). As the medial part of the hypothalamus (especially the dorsomedial hypothalamus [DMH]) is considered to be a key subcortical region associated with animals' defensive behavior and arousal states (Kataoka et al., 2020; LeDoux, 2012; Li et al., 2002; Martinez et al., 2008; Pinol et al.,

A No Rat period   Rat period

HC   NC   TC   HC   NC   TC
                    Safe   Dangerous Zone

B

C *dCA3* DAPI *c-Fos*   Housed / No Rat / Rat

D *dDG* DAPI *c-Fos*   Housed / No Rat / Rat

E c-Fos Density (cells/mm²)   Housed / No Rat / Rat

F c-Fos Density (cells/mm²)   Housed / No Rat / Rat

G HC-NC transition

H HC-NC transition

I Recording in dCA3
   Entering the NC

   No Rat period
   vs. Rat period

   HC → NC   TC
   Safe   Dangerous Zone

J No Rat

K Rat

L 137 dCA3 PI / 137 dCA3 PI / 59 dCA3 PE / 59 dCA3 PE

(legend on next page)

2018), we hypothesized that the dHPC-dLS-DMH pathway may play an active role in controlling the balance between exploratory and defensive behaviors.

We investigated the balance between exploration and defense in a semi-natural potential threat environment, in which a predatory rat was confined in the test chamber of the predator threat test (PTT) equipment (De La Flor et al., 2017; Kim et al., 2015; Ribeiro-Barbosa et al., 2005; Silva et al., 2013). In a dynamic complex threat environment, individuals show more complex behaviors, such as risk explorations (e.g., investigation of dangerous zones and avoidance) and high-risk explorations (e.g., active approach of caged predators). At the neuronal level, we identified the dCA3^{Glu}-dLS^{GABA}-DMH circuit, which responds to the exploration-defense balance in the PTT. Furthermore, optogenetic activation of this circuit induced an increase in risk exploration and a decrease in defensive behavior, while its inhibition specifically suppressed risk exploration and enhanced defensive behaviors. In addition, activation of dCA3-^{GABA} induced an extraordinary promotion of defensive response and suppression of risk exploration. Notably, activation of the dCA3^{Glu}-dLS^{GABA}-DMH circuit specifically suppressed predatory threat-evoked increases in arousal levels. Our results show that, in nature, animals adopt appropriate behaviors for the balance between defensive and explorative activities, and the dCA3^{Glu}-dLS^{GABA}-DMH circuit favors such a switch by modulating the animal's arousal state.

RESULTS

The dHPC involved in defensive and exploratory behavior

Risk exploration behavior is an intrinsically driven, active behavior process. To investigate the balance between risk exploration and defense, we adopted a PTT behavior paradigm (De La Flor et al., 2017; Kim et al., 2015; Ribeiro-Barbosa et al., 2005; Silva et al., 2013). The PTT apparatus consisted of a home chamber (HC), a narrow corridor (NC), and a test chamber (TC), in which a predatory rat was confined (Figures 1A and S1A). Only the mice, not the predatory rat, could pass through the doors and move freely throughout the apparatus (Figure 1A). The PTT contains a No Rat period followed by a Rat period (Figure S1A). During the No Rat period, the mice showed a high exploration activity throughout the entire apparatus (Figure 1A), while in the

Rat period, the presence of a predator elicited robust defensive responses (Silva et al., 2013). This was evidenced by a consistent avoidance in the HC, i.e., the safe zone (p = 3 × 10^{-8}), and decreased entries to (p = 0.034, Figures 1A and 1B) the dangerous zone (the NC and TC) and increased flight behavior (Video S1). Notably, the mice still retained a noticeable tendency to explore the dangerous zones after the emergence of a potential threat (a confined predator rat) (Figure 1B), which demonstrates the ability of risk exploration to update environmental information to meet basic resources and thus a capacity to adapt (De La Flor et al., 2017; Padilla et al., 2016). Next, we investigated the exploratory activity in response to a range of threat levels, including neutral, risk, and high-risk exploration (De La Flor et al., 2017; Dudchenko and Wallace, 2018; Padilla et al., 2016; Sturman et al., 2018) (Figures S2E–S2H, and Video S1). We observed that the mice have shown appropriate exploratory and defensive behaviors, leaving the HC and revisiting the NC to explore the environment under potential threat, and flee back to the HC afterward, leading to a repeated spatial transition between the safe and dangerous zones. During this process, the activity of risk exploration could be considered a measure of the balance between exploration and defense. Therefore, PTT offers an ideal paradigm for the quantification of the characteristics of exploratory and defensive behaviors and the relationship between them.

To identify which brain regions are engaged in contextual exploration or a predatory threat, we performed c-Fos mapping of the mouse brains after PTT (Figure S1B). Compared with the Housed (in homecage) group, samples in the PTT groups (both in No Rat and Rat periods) exhibited significantly increased c-Fos expression in a broad range of brain regions, including the dHPC (Figures 1C–1F), septum, posteroventral part of the media amygdala (MeApv), DMH, and dorsomedial part of the ventromedial hypothalamus (VMHdm), lateral hypothalamus (LH), anterior hypothalamus, and posterior hypothalamus (PH) (Figures S1C and S1D). Compared with the No Rat period, the VMH neurons were significantly activated by the presence of predators (p = 0.01609. Figure S1D), which is consistent with previous studies (Kunwar et al., 2015; Perez-Gomez et al., 2015; Silva et al., 2013). However, c-Fos expression in the dCA3 showed a significant decrease during the Rat period (dCA3, p = 3.2 × 10^{-5}; Figures 1C and 1E), suggesting that the activity of dHPC neurons (dCA3) were inhibited by the predatory rat.

Figure 1. dHPC neurons are inhibited by a potential threat

(A) Schematic representation of the PTT and examples of mouse movement traces.

(B) Quantitative comparison of defensive behavioral activities of mice (n = 18 mice).

(C and D) c-Fos expressions in the dCA3 (C) and dDG (D) in the housed, No Rat, and Rat groups, respectively. Right: enlarged view of the region in the red box. Blue, DAPI; red, c-Fos.

(E and F) Quantitative analysis of c-Fos expression in the dCA3 (E, housed, n = 6 mice; No Rat, n = 5 mice; Rat, n = 4 mice) and dDG (F, housed, n = 6 mice; No Rat, n = 4 mice; Rat, n = 7 mice).

(G and H) Representative raster plots and waveforms of a positive (G) and a negative (H) response dCA3 neuron of NC entering behavior in the Rat period.

(I) Schematic representations of NC entering behavior.

(J and K) The percentage of excited (red), inhibited (blue), and non-responsive (gray) PE (triangle, No Rat, n = 60 neurons from eight mice; Rat, n = 66 neurons from eight mice) and PI neurons (circle, No Rat, n = 139 neurons from eight mice; Rat, n = 128 neurons from eight mice) in the dCA3 during NC entering in the No Rat period (J) and Rat period (K).

(L) Distribution of NFRD of the classified dCA3 putative inhibitory neurons (dCA3 PI, 137 units) and putative excitatory neurons (dCA3 PE, 59 units) in the HC (blue) or NC (red) during the No Rat period and Rat period. Bin = 0.1. Data are presented as mean ± SD; paired t tests were used in (B); in (E and F), unpaired t tests were used; *p < 0.05, ***p < 0.005, N.S., not significant.

Driven by an instinctive exploratory nature, the experimental animals exhibited a tendency to reenter the NC from the HC to update the environmental information. To directly monitor the function of dCA3 neurons in this risk exploration behavior, single-unit recordings were conducted *in vivo* during PTT, and the responsive neurons were identified (Figures 1G and 1H). When the mouse moved from the HC to the NC (entering the NC), 47% of dCA3 putative excitatory neurons (PE) were activated (28 excited PE, 8 inhibited PE) in the No Rat period, and 50% of dCA3 PE were inhibited (33 inhibited PE, 12 excited PE) in the Rat period. In contrast, 29% of dCA3 putative inhibitory neurons (PI) were excited by entering the NC (37 excited PI, 15 inhibited PI). To further evaluate the changes in the firing of dCA3 neurons in HC and NC, we compared the distribution of the normalized firing rate difference (NFRD). We found that in the HC, most of dCA3 neuronal NFRD (93% PI, 83% PE) was concentrated within an interval between −0.2 and 0.2. In the NC during the Rat period, the NFRD of 56 (41%) PIs and 9 (15%) PEs were above 0.2, and the NFRD of 25 (18%) PIs and 27 (46%) PEs were below −0.2 (Figure 1L). In the NC during the No Rat period, the changes in the NFRD of PIs (NFRD < −0.2, 27%; NFRD >0.2, 21%) and PEs (NFRD < −0.2, 32%; NFRD >0.2, 12%) were less obvious than those in the Rat period. Furthermore, we analyzed the distribution of NFRD of the shuffled control group (Figure S1E), and we found that the rate of NFRD above 0.2 or below −0.2 was approximately 19%. Overall, the dCA3 GABAergic neurons tended to be more excited under a potential threat than they were in a neutral environment, while dCA3 glutamatergic neurons tend to be more inhibited.

dCA3 glutamatergic neurons were conversely responsive to contextual exploration and risk exploration

We further observed that the experimental mice displayed other risk exploration behaviors, including exploring at the entrance to the NC from the HC (HC door) (Video S1, Figures S2F, and S2H, 79% of risk exploration), rearing in the NC (Video S1, Figures S2F, and S2H, 21% of risk exploration), and exploring at the entrance to the TC from the NC (TC door), which were defined as high-risk explorations (Video S1, Figures S2G, and S2H). Therefore, we further analyzed the neuronal activity related to these risk exploration behaviors (Figures 2 and S2A–S2D). We found that in the No Rat period, dCA3 PE neurons were significantly excited by contextual exploration (HC door exploration, p = 0.00152; TC door exploration, p = 3.8 × 10^{-4}; Figure 2C), in accordance with our c-Fos mapping results showing that hippocampal neurons were activated by contextual exploration in the No Rat period (Figures 1C–1F, No Rat group vs. Housed group: dCA3, p = 7 × 10^{-9}; dDG, p = 2.8 × 10^{-4}). In contrast, risk exploration induced a decrease in dCA3 PE neurons (HC door exploration, p = 2.1 × 10^{-6}; Figure 2C). It is known that the hippocampus plays a key role in exploration (Berger et al., 2006; Saab et al., 2009; Wang et al., 2020); our results showed that dCA3^{Glu} neurons responded negatively to risk exploration in the Rat period, whereas dCA3^{Glu} neurons were activated by contextual exploratory behavior in the No Rat period. To clarify whether the responsive dCA3^{Glu} neurons could be included in the same population, we quantified the change in activity of dCA3 neurons when the mice were exploring at the HC door

and entering the NC both in the No Rat and Rat periods, respectively. In 60 dCA3 PE neurons, 34 units were excited by exploring at the HC door (No Rat period), 28 units (82%) were inhibited during exploration at the HC door (Rat period) (Figure 2D). Similarly, in 24 dCA3 PE neurons excited by entering the NC (No Rat period), 16 units (67%) were inhibited by entering the NC (Rat period) (Figure 2E). Directly, firing of dCA3 PE neurons significantly decreased during exploration at the HC door during the Rat period compared with the No Rat period (p = 4.9 × 10^{-6}, Figure S2B). Meanwhile, the dCA3 PI neurons did not show this phenomenon; few PI neurons were simultaneously responsive to both contextual exploration and risk exploration (Figure S2C). Taken together, there is a subpopulation of the dCA3^{Glu} neurons (∼35%) that have a positive response to contextual exploration and a negative response to risk exploration, which indicates that they may participate in the balance between exploratory and defensive behavior by changing the firing of their neurons (Figure S2D). Interestingly, activation of dCA3 PE neurons may predict further exploratory behavior, which was demonstrated by neuronal activity in mice before entering the NC (in the HC) (p = 0.03853, Figure 2C).

dCA3^{Glu} activation increases exploration and locomotion but inhibits defensive behaviors

Next, we recruited optogenetic stimulation to verify the dual function of dCA3^{Glu} neurons in defense and exploration behaviors, especially risk exploration behaviors. We found that optical activation of dCA3^{Glu} neurons produced a significant decrease in defensive behaviors and an increase in locomotion (p = 0.03093, Figure S7C), including decreasing time spent in the HC (p = 0.00143) and increasing entries into the dangerous zone (p = 8.9 × 10^{-4}, Figures 3A, 3B, and S3A). In contrast, optogenetic activation of dCA3 GABAergic neurons led to an increase in avoidance of the dangerous zone (p = 0.00249, Figure S2I) and a decrease in locomotion (p = 0.0236, Figure S7C). Furthermore, the exploratory activity of the mice was increased by dCA3^{Glu} activation in the PTT, including neutral, risk, and high-risk exploration (p = 0.03412, p = 0.00112, p = 4.7 × 10^{-4}, Figures 3C, 3D, and S3A).

We then sought to elucidate whether dCA3 influences defense and exploration behavior through the downstream LS circuitry. First, we investigated the effects of dCA3^{Glu} activation on neuronal activity in the dCA3 and other PTT-related brain areas under predatory threat via c-Fos expression after the behavioral test (Figures 3E, 3F, S3B, and S3C). Compared with the no-stim group, optical stimulation of the dCA3 neurons caused a dramatic increase in the expression of c-Fos in the dDG, dCA3, and LS, whereas decreased c-Fos expression was recorded in the DMH, MS, and LH (Figures S3B and S3C). We observed that most of the activated dDG and dCA3 neurons were glutamatergic neurons (Figures 3E and 3F), while more than 95% of the activated dLS neurons were GABAergic neurons (Figures S3D and S3E). In addition, c-Fos expression in DMH^{VGLUT+} neurons decreased by activation of dCA3^{Glu} neurons (p = 0.01321; light off group, 4.7 ± 4 cells, 19.5% ± 2.8%; light on group, 1.3 ± 2 cells, 1.6% ± 3%; Figures S3D and S3E). As the LS is one of the major projection targets of the hippocampus predominated by GABAergic neurons (>90%, Figure S3D), we hypothesized
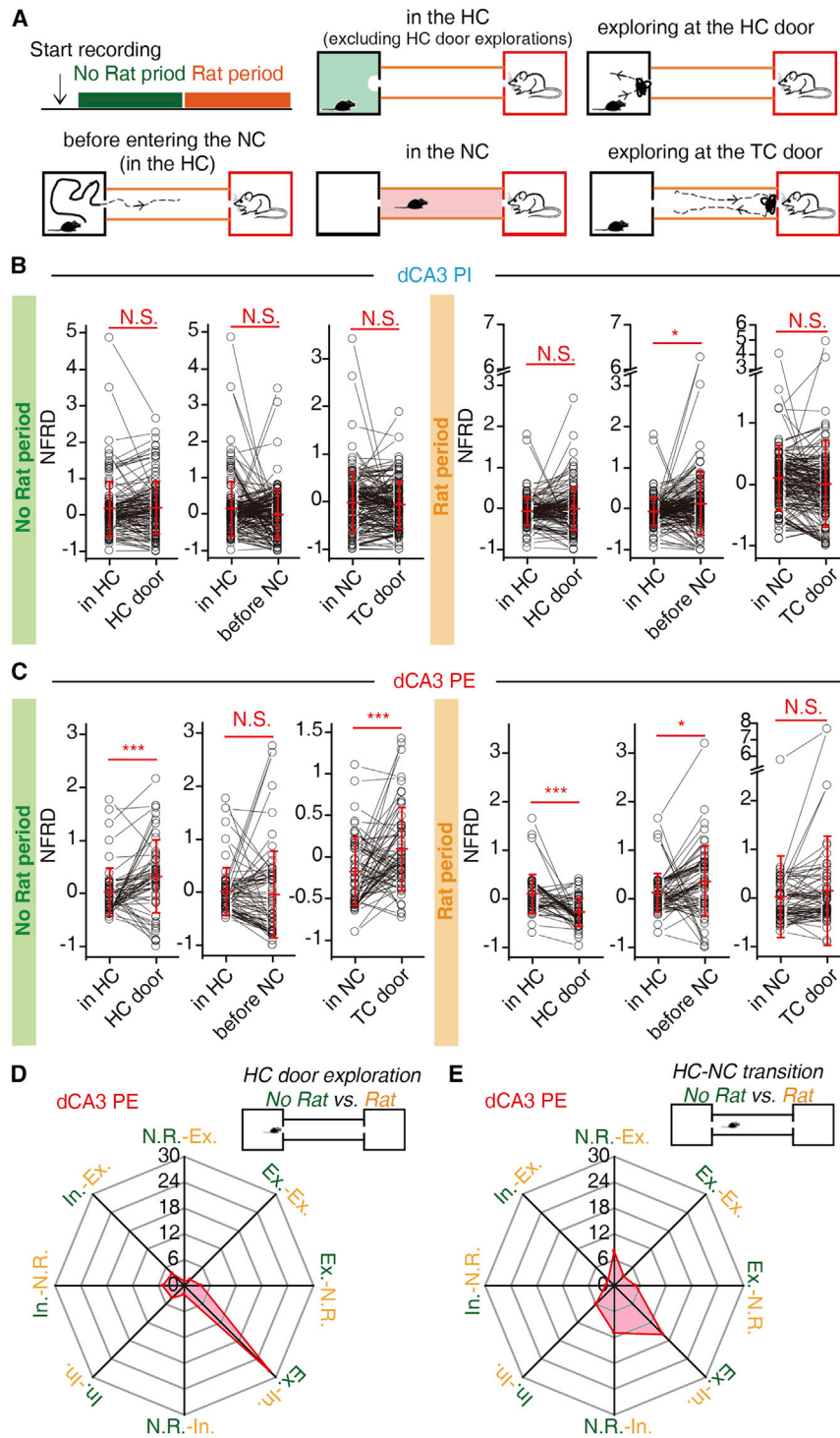
Figure 2. A subpopulation of dCA3^Glu neurons were excited by contextual explorations but inhibited by risk explorations

(A) Schematic representation of in the HC, exploring at the HC door, in the NC, before entering the NC and exploring at the TC door behaviors.

(B and C) Comparisons of NFRD of the classified dCA3 putative inhibitory neurons (B, dCA3 PI, 136 units from eight mice) and putative excitatory neurons (C, dCA3 PE, 59 units from eight mice) in the HC, exploring at the HC door, before entering the NC, in the NC and exploring at the TC door during No Rat period and Rat period of PTT.

(D and E) Radar plot representation of the dCA3 PE neuronal response to the HC door exploration (D, no response (N.R.)-N.R. = 10 units, Ex.-N.R. = 1 unit, Ex.-Ex. = 14 units, Ex.-N.R. = 4 units, Ex.-In. = 28 units, N.R.-In. = 2 units, In.-In. = 4 units, In.-N.R. = 5 units, In.-Ex. = 4 units) and upon entering the NC (E, N.R.-N.R. = 7 units, Ex.-N.R. = 8 units, Ex.-Ex. = 3 units, Ex.-N.R. = 5 units, Ex.-In. = 16 units, N.R.-In. = 11 units, In.-In. = 6 units, In.-N.R. = 2 units, In.-Ex. = 2 units) in the Rat and No Rat periods. n = 60 units from eight mice. Insert of (D): Schematic representations of the HC door exploration in the Rat and No Rat periods; insert of (E): Schematic representations of the NC entry in the Rat and No Rat periods. Excited (Ex.); inhibited (In.); N.R. Saffron, Rat period; black, No Rat period. Data are presented as mean ± SD; paired t test was used; *p < 0.05, ***p < 0.005, N.S., not significant.

that the activity of DMH neurons was suppressed by the excitation of the dCA3^Glu-dLS^GABA circuit in PTT.

Connections of the dCA3^Glu-dLS^GABA-DMH circuit

To confirm our hypothesis that the dCA3-dLS-DMH circuit dominates the regulation of exploration and defense behavior, we first verified the structural and functional connections of this circuitry. We used both anterograde (adeno-associated virus [AAV]) and retrograde (cholera toxin subunit B [CTB]) tracing techniques to identify the inputs to and outputs from the LS, observing strong direct projections from the dCA3^Glu neurons to the dLS and from the dLS^GABA neurons to the DMH (Figures S4A–S4D). Furthermore, to test whether the dHPC-dLS-DMH circuit is a dual synaptic connection, we adopted RV tracing for structural labeling (Figure 4A), and RV^+ neurons were preferentially observed in both the dLS and dCA3 (RV + neurons in dCA3 more than dCA1, p = 0.00222, Figures 4B–4D), whereas it was not observed in the dHPC in the control group (Figure S4E). These results suggest a top-down multi-synaptic circuit for dCA3^Glu-dLS^GABA-DMH.

To investigate the functional characteristics of the dCA3-dLS-DMH circuit, we combined optogenetic stimulation and multi-region electrophysiological recordings to dissect the response of DMH neuronal activity to the dCA3-dLS projections, dLS
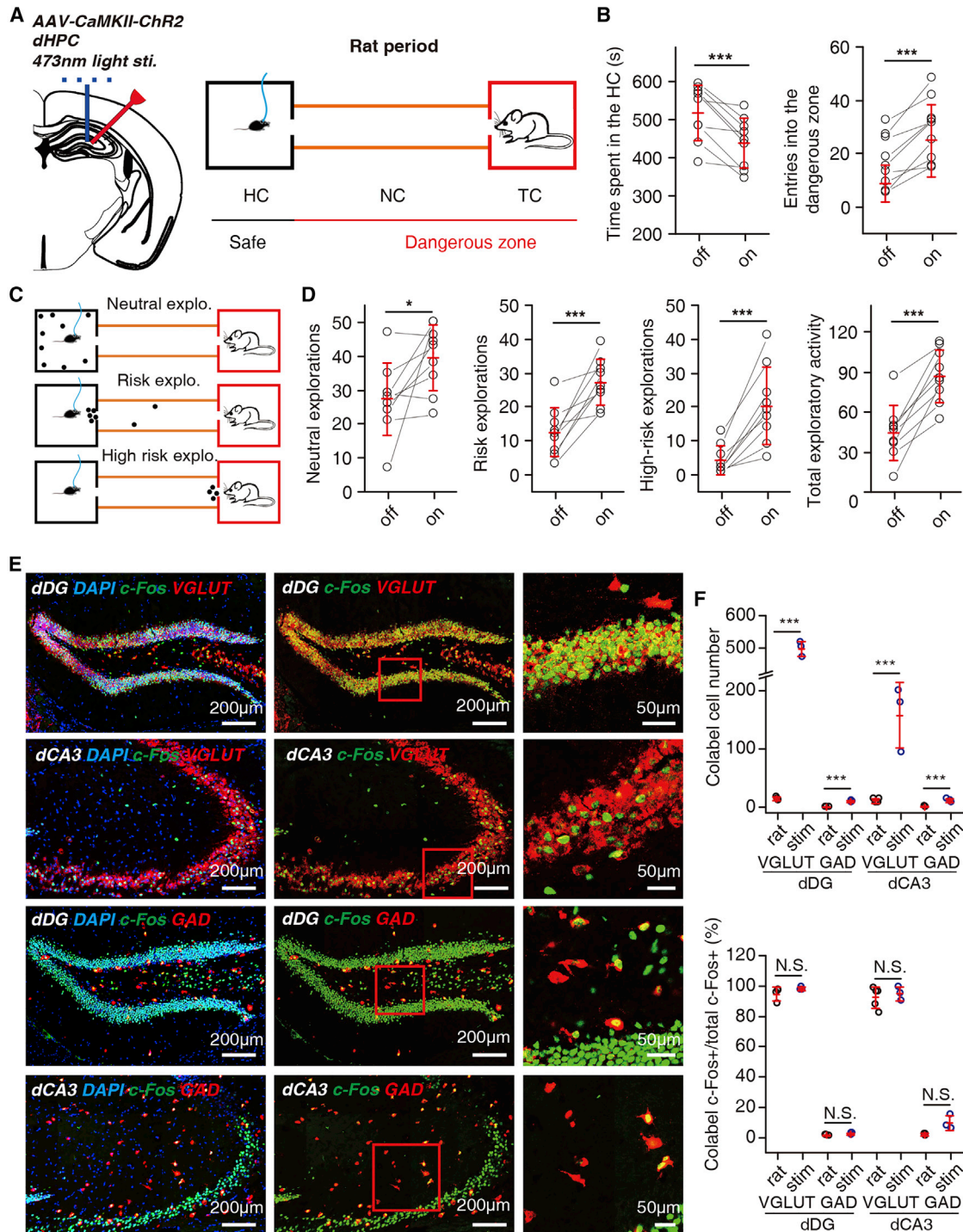
Figure 3. Activating the dCA3[Glu] neurons increases exploratory and inhibits defensive behaviors
(A) Left, targeted sites for *in vivo* optical stimulation. Right, schematic of the PTT.
(B) Defensive behavioral analysis during the activation of dCA3[Glu] neurons in the Rat period (n = 9 mice).
(C) Schematic representation of different exploratory behaviors. The dots represent the location of mice.
(D) Exploratory behavioral analysis during activation of dCA3[Glu] neurons in the Rat period (n = 9 mice).

(legend continued on next page)

neurons, or dLS-DMH projections. We observed that dCA3^{Glu}-dLS activation (20 Hz, 473 nm, 5 ms) excited 43% (59) of dLS neurons and the interspike intervals (50 ms) became more regular (Figures 4E, 4F, and S4F–S4H), suggesting a direct excitatory effect on the projected dLS^{GABA} neurons. Furthermore, dCA3^{Glu}-dLS activation resulted in profound changes in neuronal activity in the DMH, where 35% (25) of the DMH neurons was significantly inhibited and 33% (23) of them was significantly activated (Figures 4G and S4H). As shown in Figures 4E and 4F, neurons with wide half-widths tended to be more inhibited. Moreover, a previous study considered the action potential half-width of hypothalamic glutamatergic neurons to be wider (Siemian et al., 2020). Interestingly, the c-Fos expression of DMH VGlut+ neurons was decreased, while the c-Fos expression of DMH GAD+ neurons was increased by activation of the dCA3^{Glu} neurons in the PTT (Figures S3D and S3E). These results demonstrate that neuronal activity in the DMH can be functionally modulated via dCA3^{Glu}-dLS excitation, and DMH^{Glu} may be the target of the dCA3^{Glu}-dLS pathway.

Moreover, we studied the functional response of DMH neurons to dLS^{GABA} activation and dLS^{GABA}-DMH projection activation. We observed that direct activation of dLS^{GABA} neurons caused increased activity in 45% (44) of DMH neurons (Figures S4J–S4M). Interestingly, activating the dLS^{GABA}-DMH projections resulted in the inhibition of 35% (36) of the DMH neurons (wide half-width neurons tend to be inhibited) and the excitation of 36% (37) of the DMH neurons (Figures 4H, 4I, and S4I); recall that this result is similar to the neuronal responses during dCA3^{Glu}-dLS activation. From these results, we can infer that both dCA3^{Glu}-dLS and dLS^{GABA}-DMH projections can produce similar effects to DMH neurons. Therefore, these results verify the existence of a connection, both anatomic and functional, between the dCA3 and DMH, which proved our hypothesis that the dLS^{GABA}-DMH pathway can process information from dCA3^{Glu}, including defensive and exploratory behaviors.

dLS and DMH neurons were responsive to risk exploration in the rat period of the PTT

To directly verify whether dLS and DMH participate in processing threat context information in the Rat period, we monitored the neuronal activity of dLS and DMH in free-behaving mice during the Rat period (Figures 5 and S5). We analyzed these two brain areas firing in the NC and after fleeing behaviors. We found that 22% (20) of the dLS^{GABA} neurons were inhibited by entering the NC (Figure 5B), whereas 28% (25) of the dLS^{GABA} neurons were excited after the mice stopped fleeing (Figure S5), suggesting that the activity of dLS^{GABA} neurons was primarily suppressed by threat. Furthermore, 23% (25) of DMH neurons responded positively to entering the NC (Figure 5C), whereas 18% (18) of DMH neurons showed a negative response after fleeing behavior (Figure S5). As previous studies have suggested that neurons in subcortical brain regions can be classified according to the fre-

quency of firing rate of electrophysiological properties (Siemian et al., 2020; Trenk et al., 2022), we classified neurons in the dLS and DMH according to firing rates. We then analyzed different types of neurons in response to different risk exploration behaviors, and the results are shown in Figures 5F–5I and S5. Notably, we found that dLS class II neurons (firing rates >2 Hz) were significantly decreased (2 dLS class II neurons NFRD >0.2, and 22 dLS class II neurons NFRD < −0.2; p = 2.6 × 10^{-4}; Figure 5G) and DMH class I neurons (firing rates <2 Hz) were significantly increased (17 DMH class I NFRD >0.2, 11 DMH class I NFRD < −0.2; p = 0.035; Figure 5I) in the NC compared with the HC in the Rat period. Moreover, dLS class II neurons (firing rates >2 Hz) also were suppressed by flight (p = 1.1 × 10^{-5}) and risk exploration (exploring at the HC door, p = 0.045). DMH class I neurons were increased by flight behavior (p = 0.0012), and DMH class II neurons were increased by risk exploration (exploring at the HC door, p = 0.0032). These results demonstrated that predator threat inhibits high-frequency dLS class II neurons while exciting low-frequency DMH class I neurons. Taken together, the dCA3^{Glu}-dLS^{GABA}-DMH circuit may be inhibited by predator-induced risk information, which is involved in the regulation of defensive and risk exploratory behaviors.

Activating the dCA3^{Glu}-dLS^{GABA}-DMH circuitry inhibits defensive behaviors and increases risk exploration specifically

To further verify the role of the dCA3^{Glu}-dLS^{GABA}-DMH circuit in exploratory and defensive behaviors, we activated dLS-projecting dCA3^{Glu} neurons and DMH-projecting dLS^{GABA} neurons, respectively (Figures 6 and S6, and Video S2). Consistently, we found that the defensive behaviors, including time spent in the HC and entries into the dangerous zone, were significantly decreased by activation of dCA3^{Glu}-dLS projections (p = 6.4 × 10^{-4}; p = 6.0 × 10^{-5}; Figures 6B, S6A, and S6B), and the time spent in the HC was significantly decreased by activation of the dLS^{GABA}-DMH pathway (p = 0.0147; p = 0.0815; Figures 6E, S6D and S6E).

Moreover, we also analyzed the influence of the activation of dCA3^{Glu}-dLS^{GABA}-DMH circuit on the exploration behavior in the PTT Rat period. Our experiments revealed that dCA3^{Glu}-dLS activation increased exploratory activity (p = 1.0 × 10^{-4}, Figures 6C and S6C), especially the risk explorations (p = 0.00132) and high-risk explorations (p = 9.3 × 10^{-5}), but did not affect the neutral explorations (p = 0.53982) and locomotion (p = 0.6212, Figure S7D). In accordance with the results of dCA3^{Glu} activation, this implies that risk exploration can suppress defensive behavior. During optical stimulations of the dLS^{GABA}-DMH, the activity of exploratory behaviors (p = 0.283, Figure 6F), including neutral explorations (p = 0.50237) and risk explorations (p = 0.61306), remained unchanged. In addition, the locomotion significantly decreased, while the high-risk explorations increased (p = 0.03074). Furthermore, we recruited optogenetic inhibition to further confirm the

---

(E) Left and middle, co-localization of c-Fos-positive neurons with VGLUT-positive or GAD-positive neurons in the dDG and dCA3 of mice after the PTT; Right, enlarged view of the region in the red box. Blue, DAPI; green, c-Fos; red, VGlut or GAD.

(F) Quantification of the co-localization levels of c-Fos-positive neurons with GAD-positive or VGLUT-positive neurons in the dCA3 and dDG Rat group: dDG, VGlut/c-Fos$^+$, n = 5 mice; GAD/c-Fos$^+$, n = 3 mice; dCA3, VGlut/c-Fos$^+$, n = 4 mice; GAD/c-Fos$^+$, n = 3 mice; Stim group: n = 3 mice. Data are presented as mean ± SD; in (B and D), paired t tests were used; in (F), unpaired t tests were used; *p < 0.05, ***p < 0.005, N.S., not significant.
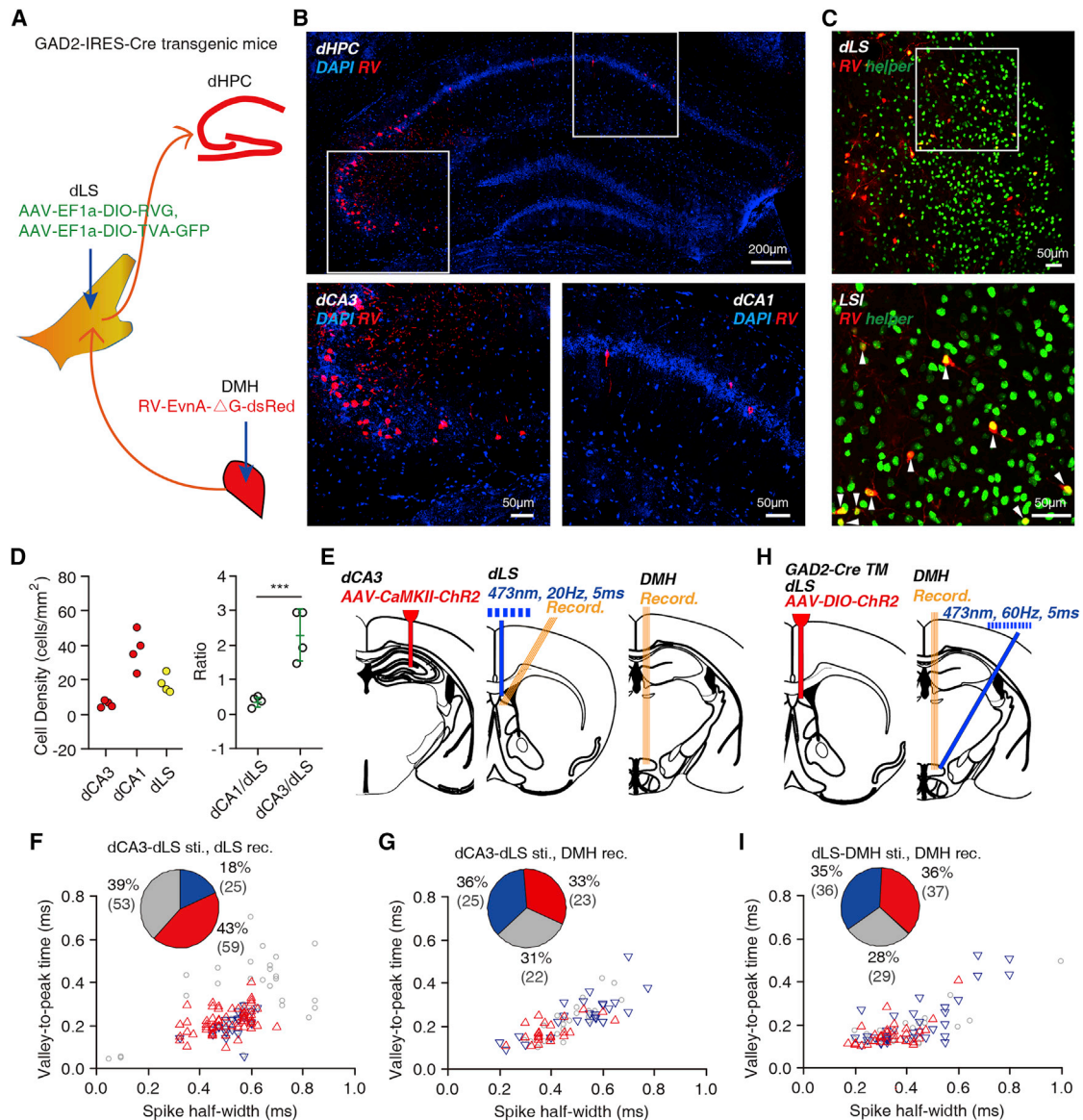
Figure 4. Anatomic and functional connections in the disynaptic dCA3^{Glu}-dLS^{GABA}-DMH circuit

(A) Schematic representation of the experimental design.

(B and C) The (B) dHPC and (C) dLS in GAD-Cre transgenic mice after the injection of the AAV-helper and RV- $\triangle$ G in the dLS and DMH, respectively. The white arrowhead indicates the start neurons (C), Blue, DAPI; red, RV; green, AAV-helper.

(D) Left, the number of RV-positive neurons in the dCA3, dCA1 and co-labeled AAV-helper and RV neurons (start cell) in the dLS. Right, the ratio of RV-positive neurons in the dCA3, dCA1 and start cell in the dLS. n = 4 mice.

(E) The optical stimulation of dCA3^{Glu}-dLS projections and electrophysiological recording in the dLS and DMH.

(F and G) The percentage of excited (red triangle) and inhibited (blue triangle) and non-responsive neurons (gray circle) in the dLS (F, n = 137 neurons) and DMH (G, n = 70 neurons) during activation of dCA3^{Glu}-dLS projections. n = 10 mice.

(H) The optical stimulation of dLS^{GABA}-DMH projections and electrophysiological recording in the DMH.

(I) The percentage of excited (red triangle), inhibited (blue triangle) and non-responsive neurons (gray circle) (n = 102 neurons) in the DMH during activation of dLS^{GABA}-DMH projections. n = 7 mice. Data are presented as mean ± SD. Paired t tests were used, ***p < 0.005.

results (Figures S6G–S6L). We found that inhibition of the dCA3^{Glu}-dLS^{GABA}-DMH circuit induced increase of defensive responses and decrease of risk explorations, but not the neutral explorations. In sum, the results are in accordance with the electrophysiological and behavioral data described above.

Controlling balance between the defensive and exploratory behaviors

Furthermore, to study the influence of the dCA3^{Glu}-dLS and dLS^{GABA}-DMH activation on predator-induced changes in arousal levels, we monitored the effects of both optogenetic
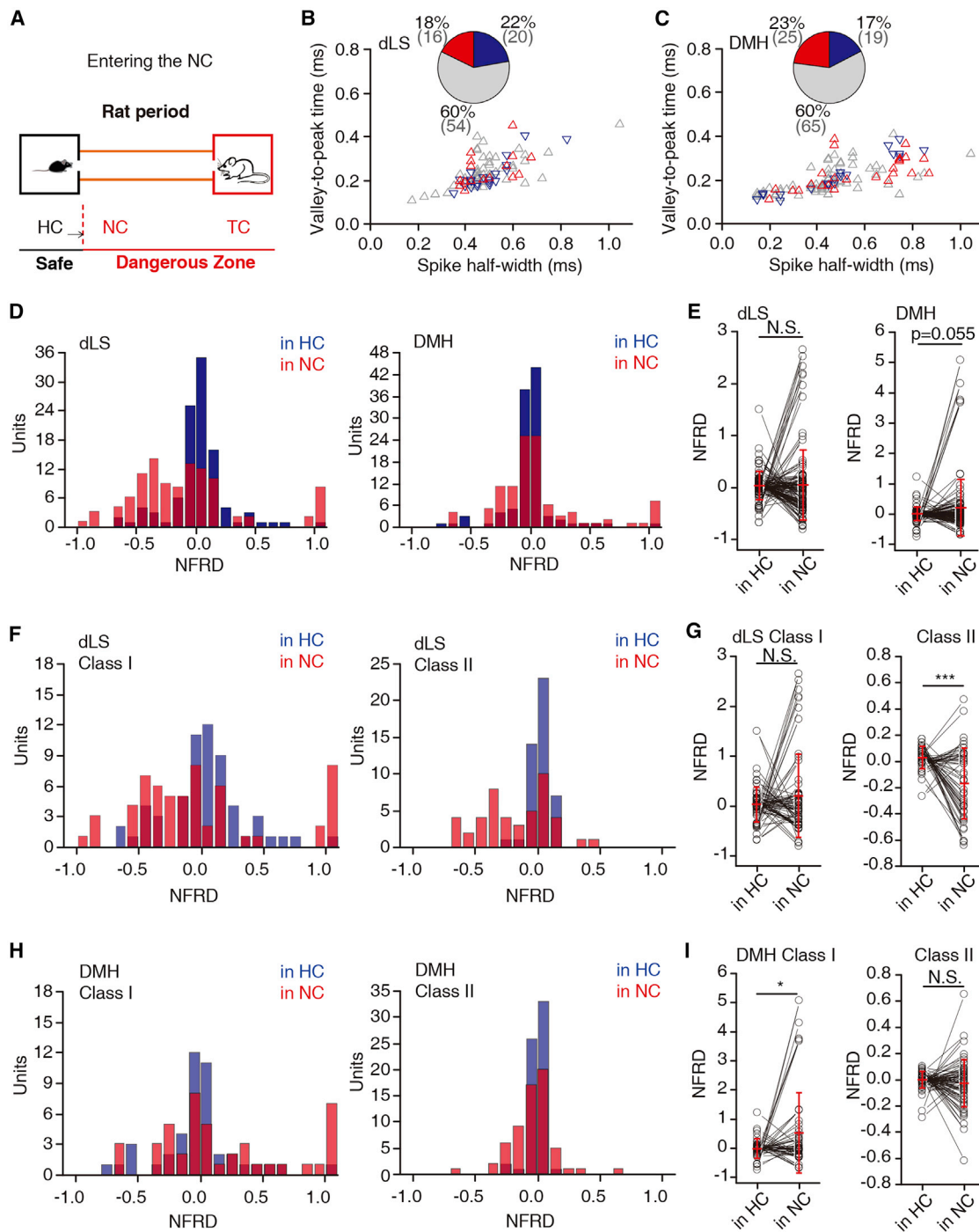
Figure 5. Threat inhibits high-frequency dLS neurons and excites low-frequency DMH neurons

(A) Schematic representation of NC entering behavior and electrophysiological recording in the Rat period of the PTT.

(B and C) The percentage of excited (red), inhibited (blue) and non-responsive (gray circle) neurons (triangle, n = 90 neurons from five mice) in the dLS (B) and DMH (C) while entering the NC.

(D and E) Distribution (D) and comparisons (E) of NFRD of the dLS (left, 105 units) and DMH (right, 107 units) neurons in the HC or NC during the Rat period of PTT.

(F and G) Distribution (F) and comparisons (G) of NFRD of dLS class I (left, 59 units) and class II (right, 44 units) neurons in the HC or NC during Rat period of PTT.

(H and I) Distribution (H) and comparisons (I) of NFRD of DMH class I (left, 46 units) and class II (right, 63 units) neurons in the HC or NC during Rat period of PTT.

Data are presented as the mean ± SD, and paired t tests were used, *p < 0.05, **p < 0.01, ***p < 0.005. N.S., not significant.
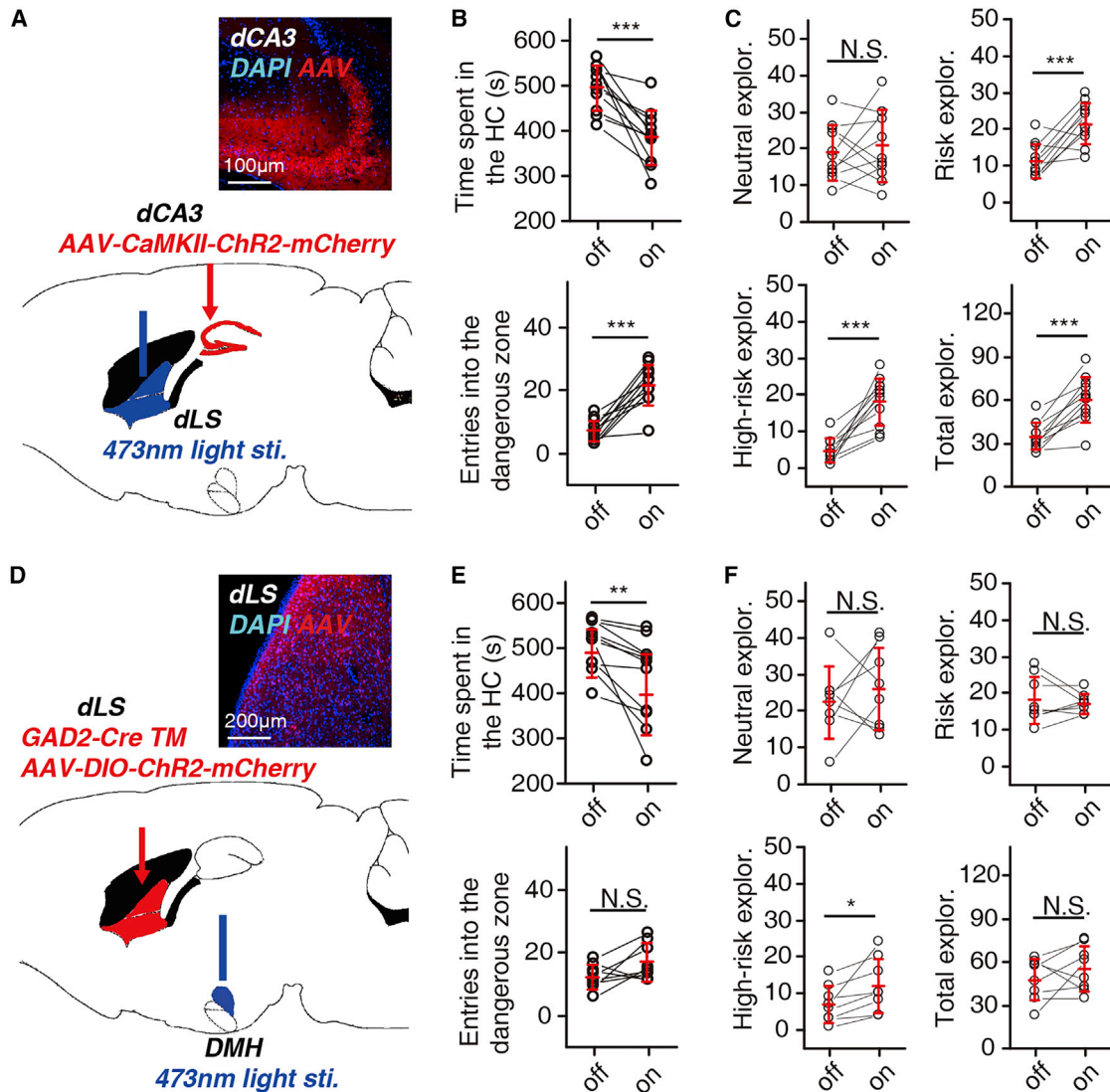
Figure 6. Optogenetic activation of dCA3^Glu-dLS^GABA-DMH circuitry inhibits defensive behavior and increases risk exploration
(A) Experimental design schematic and representative image. Red, AAV virus; blue, DAPI.
(B and C) Behavioral analysis of defenses (B) and explorations (C) before and during the activation of dCA3^Glu-dLS projections in the Rat period (n = 11 mice).
(D) Diagrams showing virus injection into the dLS and optical stimulation in DMH.
(E and F) Behavioral analysis of defenses (E) and explorations (F) before and during the activation of dLS^GABA-DMH projections in the Rat period (n = 8 mice). Data are presented as the mean ± SD, and paired t tests were used, *p < 0.05, **p < 0.01, ***p < 0.005. N.S., not significant.

activation and predator exposure on the heart rate of the mice (Figures 7A–7D). As shown in previous studies, the heart rate is one physiological measurement of emotional arousal level in free-living animals (Anderson and Adolphs, 2014; Wascher, 2021). Our results showed that the heart rate of mice that were behaving freely increased sharply upon exposure to the predatory rat (p = 0.028; p = 6.3 × 10^−4; Figure 7C), but returned to their normal levels following optogenetic stimulation of dCA3^Glu-dLS or dLS^GABA-DMH (p = 0.0041; p = 0.0033). This indicates that both dCA3^Glu-dLS and dLS^GABA-DMH activation can eliminate the upregulation of the predator-evoked arousal level. Moreover, to examine the impact of this pathway on the arousal level of animals, we monitored the heart rate of anesthetized

mice before and during optogenetic stimulation (Figure 7D). We observed that dLS^GABA-DMH projection activation directly suppressed mouse heart rate (p = 0.02739), whereas dCA3^Glu-dLS activation did not affect heart rate (p = 0.37493). This implies that the DMH, as the terminal of the dCA3^Glu-dLS^GABA-DMH circuit, may act as an effector that individuals' exploratory behavior suppresses defensive behaviors.

To further investigate the relationship between exploratory and defensive behaviors during the Rat period, we calculated the correlation between the defensive avoidance score (time spent in the HC divided by the duration of the Rat period) and the exploratory activities (Figures 7E and S7), observing a negative correlation between the avoidance score and total
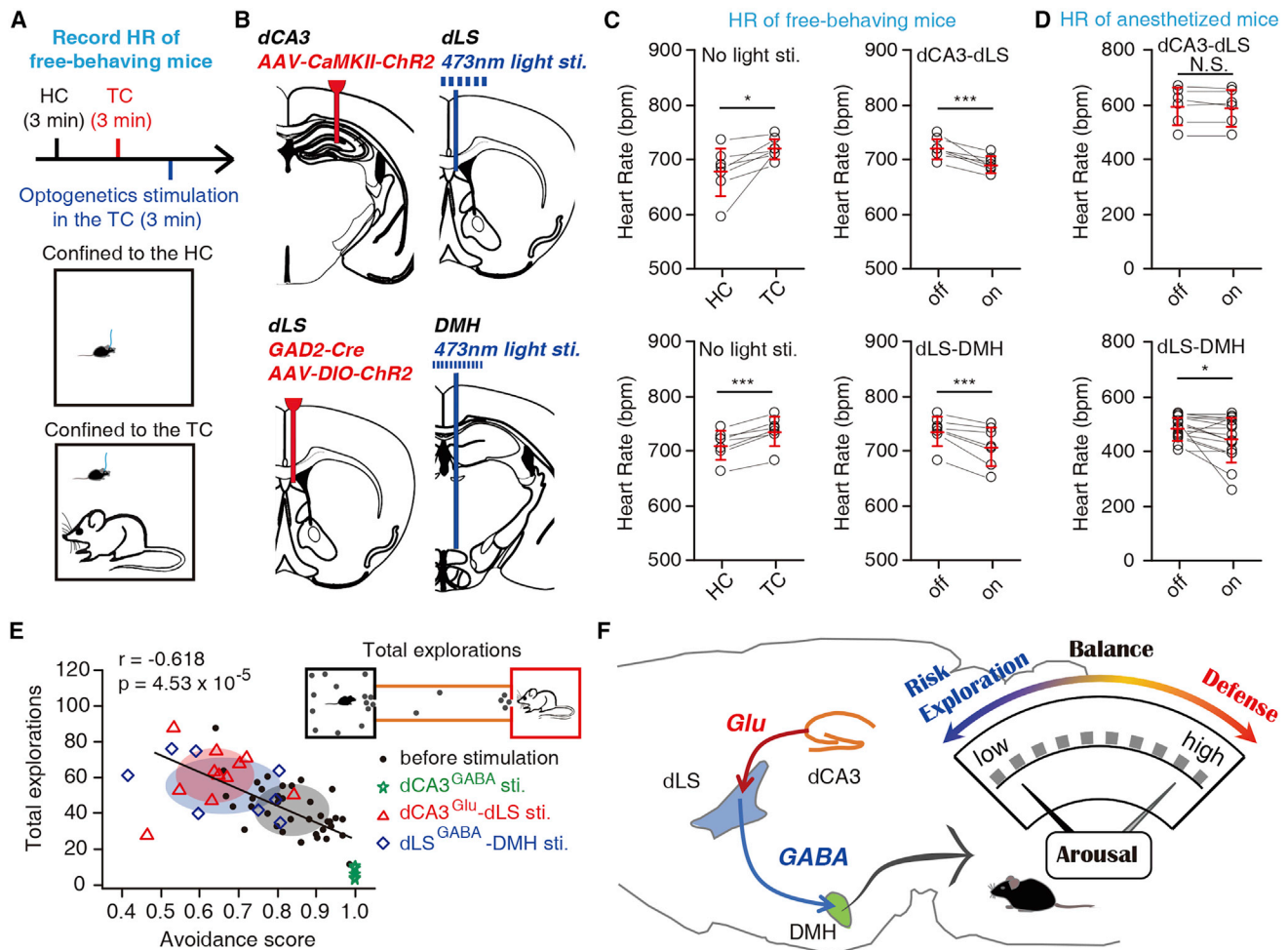
Figure 7. Activation of the dCA3-dLS-DMH circuit mediates balance between defense and exploration

(A) Experimental paradigm for heart rate recording in free-behaving mice.

(B) Top, Diagrams showing virus injection into the dCA3 and optical stimulation in dLS; down, diagrams showing virus injection into the dLS and optical stimulation in DMH.

(C) The heart rates of mice were measured both in the HC and in the TC, as well as optogenetic activation of dCA3^{Glu}-dLS or dLS^{GABA}-DMH projections during in the TC (n = 7 mice).

(D) In anesthetized mice, heart rates were measured during optical stimulation of dCA3^{Glu}-dLS or dLS^{GABA}-DMH projections (top, n = 6 mice; bottom, n = 16 mice).

(E) The correlation between total explorations and avoidance score during non-stimulation (n = 37 mice), dCA3^{GABA} stimulation (n = 6 mice), dCA3^{Glu}-dLS stimulation (n = 11 mice), and dLS^{GABA}-DMH stimulation (n = 8 mice). The avoidance score was calculated as the time spent in the HC divided by the entire Rat period duration (600 s).

(F) Proposed model for the dCA3^{Glu}-dLS^{GABA}-DMH circuit. Data are presented as mean ± SD. Paired t test was used; *p < 0.05, ***p < 0.005, N.S., not significant.

exploratory activities in the Rat period of PTT. Moreover, the defensive avoidance score negatively correlated with the risk exploratory activities (Figures S7F and S7G), including risk explorations and high-risk explorations. However, no significant correlation was observed between the defensive avoidance score and neutral exploration (Figure S7H). Activation of the dCA3^{Glu}-dLS and dLS^{GABA}-DMH shifted the animals' behavior toward higher exploration and lower defense, whereas activation of the dCA3 GABAergic neurons shifts the animals' behavior toward lower exploration and higher defense. The correlation between exploration in the HC and avoidance score was negative, implying that the number of explorations does not increase with

the time spent in a particular area during PTT. Taken together, our results imply a competitive relationship between exploratory and defensive behaviors, and the dCA3^{Glu}-dLS^{GABA}-DMH circuit may be involved in controlling these transitions within an appropriate range.

Besides, we investigated the influence of the dCA3^{Glu}-dLS^{GABA}-DMH activity on motion (Figures S7A–S7E). We used open field test behavior and optogenetics to verify this and found that activation of dCA3^{Glu} neurons significantly increased animal locomotion (p = 0.0309), and activation of dCA3^{Glu}-dLS projection had no significant influence on animal locomotion (p = 0.6212), while activation of dLS^{GABA}-DMH projections

significantly decreased animal locomotion (p = 0.0078). Moreover, we found that both activation of dCA3 VGAT + neurons and inhibition of dCA3^{Glu}-dLS projections suppressed animal movement (p = 0.0236; p = 0.0017). Taken together, the dCA3^{Glu}-dLS^{GABA}-DMH circuit specifically related to risk exploration and defense, but not to neutral exploration or movement. In summary, we hypothesized that under normal circumstances, the dCA3^{Glu}-dLS^{GABA} pathway is activated by contextual exploration, and dLS^{GABA} appropriately inhibits DMH activity to a baseline level, while arousal levels are normal. When a risk cue was detected, the activity of the dCA3^{Glu}-dLS^{GABA} pathway was inhibited, which subsequently weakened the suppression effect of dLS^{GABA} projections and led to an abnormal increase in DMH activity. As a consequence, the arousal level was increased, resulting in elevated defense behaviors, including flight and avoidance responses (Figure 7F). In contrast, activation of the dCA3 GABAergic neurons may inhibit the dCA3^{Glu}-dLS^{GABA}-DMH circuit and lead switch from exploration to defense. Thus, the dCA3^{Glu}-dLS^{GABA}-DMH circuit is involved in maintaining an individual's defensive and exploratory behaviors.

DISCUSSION

In this study, we identified a disynaptic dCA3^{Glu}-dLS^{GABA}-DMH circuit that controls exploration and defense balances in complex environments with potential threats. Our results show that dCA3^{Glu} neurons regulate both risk exploration and defensive behaviors in a potential threat environment, adding direct evidence at the cellular level to support the previous studies that dCA3 mediates exploratory behavior (Berger et al., 2006) and processes threat-conditioned context information (Besnard et al., 2020). Furthermore, we determined that the dLS, which transforms hippocampal cognitive information of the environment to subcortical action-executing regions (Bender et al., 2015; Leroy et al., 2018; Luo et al., 2011; Sweeney and Yang, 2015, 2016; Tingley and Buzsaki, 2018), is a key node that receives dCA3^{Glu} projections and, in turn, sends massive long-range projecting GABAergic terminals to the DMH. As previous research suggests that the DMH responds to stressful predator stimuli (Kataoka et al., 2020), we uncovered that the responsive DMH low-firing-rate neurons were majorly activated by threat. Collectively, this work describes a hippocampal-hypothalamic neural circuit, dCA3^{Glu}-dLS^{GABA}-DMH, which maintains appropriate defensive-exploratory behavioral outputs by mediating animals' arousal state in a complex potential risk context, updating current knowledge of interactions between survival behaviors in an ambiguous threat environment, otherwise a determinant threat context.

In nature, risk exploration and defense are critical to individuals in order to adapt to the dynamics of prey-predator co-existence across species (Berlyne, 1966; De La Flor et al., 2017; Glaudas et al., 2006; Padilla et al., 2016; van Kampen, 2015). Generally, risk exploration allows individuals to gather information about their surrounding environment (De La Flor et al., 2017; Gottlieb and Oudeyer, 2018; Gottlieb et al., 2013), including novel features and safety boundaries. In essence, it is the basis for obtaining the required resources (Mobbs et al., 2018; Padilla et al., 2016), such as water, food, mates, and shel-

ter, so that risk exploration is vital for survival and reproduction. As risk exploration is an active exploratory behavior in an ambiguous risk environment, we recruited the confined predator as a potential threat, and experimental animals were allowed to avoid the predator in the HC, actively exploring the NC and approaching the caged predator in our behavior test (Besnard et al., 2019; Kim et al., 2015; Padilla et al., 2016; Silva et al., 2013). In the semi-naturalistic apparatus, a previous study found that dCA1 place cells participate in coding the predatory threat context (Kim et al., 2015). More evidence from other labs revealed that the dHPC was considered dominant in neutral exploration, including DG, CA3, CA2, and CA1 (Berger et al., 2006; Saab et al., 2009; Wang et al., 2020). In this study, we used free-moving electrophysiological recordings to directly monitor neuronal activity (Ahmadlou et al., 2021) during spontaneous exploratory behaviors in a semi-naturalistic environment at the single-cell level, with high temporal resolution. In light of recent research, our findings indicate that a subpopulation of dCA3^{Glu} neurons (~35%), which are probably dLS-projecting neurons, can distinctively respond to neutral and risk explorations as well as defensive behaviors.

Notably, during exploration in a dynamic environment, with the emergence of a predator, individuals must quickly terminate exploration and initiate defensive behavior to avoid harm or even death (Evans et al., 2019; Headley et al., 2019; LeDoux, 2012). Animals resolving conflict between defense and risk exploration rely on integrating information from internal states and their environment (Evans et al., 2019; Headley et al., 2019; Mobbs et al., 2018). To the best of our knowledge, no evidence has been reported on the underlying neural circuits controlling the balance between exploration and defense. Previous studies on conditioning fear have shown that the hypothalamus and amygdala play key roles in the processing of defensive behavior (Cezario et al., 2008; Esteban Masferrer et al., 2020; Kitamura et al., 2017; Silva et al., 2013). Accordingly, we focused on the subcortical targeted circuit of dCA3 to support the selection of behavioral outcomes of exploration and defense, while we found that optogenetic activation of dCA3^{Glu} neurons not only led to increases in exploratory behaviors, but also decreased predator-induced defensive responses. The LS is the key relay from the dHPC to the hypothalamus to receive and transform neutral and threat contextual information from the dHPC (Besnard et al., 2019; Tingley and Buzsaki, 2018), as well as environmental explorations (Berger et al., 2006). Consistent with this view and in addition to its role in active risk exploration in a threat environment, we found that approximately 22% to 28% of the putative dLS^{GABA} neurons were suppressed by the dangerous zone in the PTT Rat period. As such, our findings demonstrate that the dCA3-dLS pathway performs the transformation of risk exploration information and benefits to resolve the two conflicting behaviors of risk exploration and defense, but not neutral exploration or movement (Table 1).

The arousal state, mediated by a broad range of brain areas, such as the hypothalamus, thalamus, and locus coeruleus, could alter defensive behavior outcomes. Specifically, in a complex semi-naturalistic apparatus, we observed that individuals who were aware of potential predatory threat display risk exploration, compelling defensive avoidance behavior and visiting

dangerous zones, and then up-regulate animals' physiological and emotional arousal levels, often following a defensive escape behavior, which is consistent with previous studies (Evans et al., 2019; LeDoux, 2012; LeDoux and Daw, 2018; Tovote et al., 2015). Our findings also directly confirmed that the animal's arousal level was increased by predatory threat (Johnson et al., 2010; Kataoka et al., 2020; Pinol et al., 2018; Zelikowsky et al., 2018). Notably, activation of dCA3^{Glu}-dLS projections suppressed the predator-evoked increasing arousal level but did not affect the arousal state of anesthetic animals, suggesting that the dCA3^{Glu}-dLS circuit may directly modulate the threat-induced change of arousal state. Previous research indicates that the hypothalamus, a major downstream component of LS, is the action execution center in defensive behaviors, compared with the emotional center amygdala (Gross and Canteras, 2012). It is important to note that DMH is considered as one of the arousal centers, modulating individuals' instinctual physiological responses (Pinol et al., 2018), including body temperature, energy expenditure, heart rate, and defensive response (Johnson et al., 2010; Zelikowsky et al., 2018). Our data indicate that DMH appears to control changes in emotional arousal level during risk exploration and defensive escape balance. We first identified a disynaptic dCA3^{Glu}-dLS^{GABA}-DMH connection and found that the low-firing-rate DMH neurons were significantly activated by the risk environment in the PTT Rat period.

Notably, previous studies have reported the involvement of the dHPC in both exploration and locomotion (Bender et al., 2015; Fanselow and Dong, 2010; Wang et al., 2020). Although we found that dCA3 activation significantly increased animal locomotion in an open field, dCA3-dLS activation did not show a similar response. Furthermore, dLS-DMH activation significantly decreased animal locomotion in an open field, most likely caused by the decreased physiological level during DMH regulation (Pinol et al., 2018). Increasing (or decreasing) locomotion activity may theoretically increase (or decrease) the entries to each zone during behavioral tests; however, it would not affect the proportion of time spent in each zone. As the time spent in the dangerous zone, explorations at the HC and TC doors during dCA3, dCA3-dLS, and dLS-DMH activations were significantly increased. However, we found no relationship between locomotion activity and defensive or risk exploratory behaviors.

Furthermore, optogenetic activation of the dLS^{GABA}-DMH circuit not only modulates the balance between risk exploration and defense, but also suppresses the predator-induced promoting arousal states, as measured by heart rates, which was one physiological measurement for monitoring emotional arousal level (Anderson and Adolphs, 2014; Wang et al., 2018; Wascher, 2021; Zhu et al., 2019). This indicates that the DMH is the effector of the dCA3^{Glu}-dLS^{GABA} circuit, which accepts the integrated environmental information to modulate emotional arousal states, and finally controls the behavior response to potential threats. As the hypothalamic structure is the major action-executing target of the hippocampal-lateral septal circuit, the LH and VMHvl were found to regulate the speed of movement (Bender et al., 2015), feeding behaviors (Sweeney and Yang, 2015, 2016), and conspecific aggression behaviors (Leroy et al., 2018; Wong et al., 2016), respectively. The LS^{GABA} neurons transfer contextual information to mediate the activity of subcortical regions,

thereby modulating behaviors such as anxiety (Anthony et al., 2014) and feeding (Carus-Cadavieco et al., 2017), whereas we emphasize that the LS^{GABA} neurons translate threatening environmental information delivered from dCA3^{Glu} to DMH to modulate the outcome of the exploration-defense behaviors. Notably, we suggest that DMH glutamatergic neurons regulate the arousal state to indirectly modulate behavioral outcomes. Next, we should uncover how DMH^{Glu} neurons functionally participate in it. In addition, risk exploration and defensive response show flexibility to potential threat contexts, including adjusting the speed of an organism dynamically as the change of other internal states, such as emotion (anxiety) and drive (hunger). As such, the long-range projecting GABAergic neurons in the LS are critical for mediating brain internal states via hypothalamic structures, and future studies should uncover the crosstalk between hippocampus-lateral septum-hypothalamic circuits (such as HPC-LS-DMH, LH, or -VMH pathways) in survival behaviors.

In summary, the dCA3^{Glu}-dLS^{GABA}-DMH circuit controls the balance between exploration and defense, maintaining adaptable and changing characteristics of defensive and exploratory strategies in a natural complex risk environment. It should be noted that optogenetic activation of dCA3^{Glu}-dLS^{GABA} and dLS^{GABA}-DMH projections led to significantly decreased defensive behaviors and increased risk of exploratory activity. In contrast, activation of dCA3^{GABA} neurons and inhibition of the dCA3^{Glu}-dLS^{GABA}-DMH circuit had the opposite effect, leading to extraordinary defensive avoidance of the caged predator and a specific decrease in risk exploration. In the future, we need to further clarify the spatiotemporal coding mechanism of this circuit for controlling the balance between exploratory and defensive behavior, including the determination of which subtype of dCA3^{GABA} neurons are responsible and how they work together with dCA3^{Glu} neurons. Remarkably, the over-excitation or inhibition of dCA3^{GABA} or dCA3^{Glu}-dLS^{GABA}-DMH circuit can bidirectionally mediate the balance of exploration and defense to abnormal range, which implies that dysregulation of this hippocampal-septo-hypothalamic circuit leads to abnormal behavioral phenotypes. Therefore, elucidating the fundamental processes of this circuit will provide insights into the possible mechanisms underlying the related neuropsychiatric diseases in humans, such as anxiety, neophobia, and post-traumatic stress disorder.

Limitations of the study

In this study, we used *in vivo* physiological recording and optogenetics to dissect the function of the dCA3^{Glu}-dLS^{GABA}-DMH circuit in the balance between defense and risk exploration, but their precise neuronal subpopulations in the circuit are still unclear. We found that DMH low-frequency class I neurons show a broader half-width than that of class II neurons, which agrees with prior reports of the electrophysiological character of hypothalamic glutamatergic neurons (Siemian et al., 2020). In comparison, DMH high-frequency class II neurons exhibited a narrower half-width, indicating that they may be GABAergic neurons. Moreover, as the dLS is dominated by different subtypes of GABAergic neurons, including somatostatin, parvalbumin, and calbindin neurons, the low-frequency dLS class I

neurons and high-frequency dLS class II neurons may belong to different subtypes defined in prior studies (Letzkus et al., 2015; Markram et al., 2004; Naka and Adesnik, 2016). However, more evidence is needed to support our inferences and further dissect the functions of the different types of neurons mentioned above. The role of specific subtypes in the dCA3^{Glu}-dLS^{GABA}-DMH circuit in related brain disorders requires further confirmation in disease models, which are open for investigation in future studies.

STAR★METHODS

Detailed methods are provided in the online version of this paper and include the following:

- KEY RESOURCES TABLE
- RESOURCE AVAILABILITY
    - Lead contact
    - Materials availability
    - Data and code availability
- EXPERIMENTAL MODEL AND SUBJECT DETAILS
    - Animals
- METHOD DETAILS
    - Virus injections
    - Fabrication of implants
    - Implantation surgery and optogenetics
    - Predator threat test (PTT) and behavioral analysis
    - Open field test (OFT)
    - Electrophysiological recordings
    - Electrophysiological data analysis
    - Histology
    - Immunohistochemistry for c-Fos protein
    - Heart rate (HR) measurements
- QUANTIFICATION AND STATISTICAL ANALYSIS

SUPPLEMENTAL INFORMATION

Supplemental information can be found online at https://doi.org/10.1016/j.celrep.2022.111570.

AUTHOR CONTRIBUTIONS

C.Z., L.L.W., Y.L., and L.P.W. designed the study and wrote the manuscript. C.Z., L.L.W., Y.C., J.Y.H., X.F.W., S.W.P., S.Y.H., and Y.L. conducted surgeries, optogenetics, behavioral experiments, immunohistochemistry, and cell counting. C.Z., C.Y.S., and Y.C. performed behavioral and electrophysiological experiments. C.Z., L.L.W., Z.H.L., X.F.W., and F.Q.X. conducted neuroanatomical tracing and in situ hybridization. C.Z., K.H., L.L.W., Y.C., C.Y.S., and Y.L. analyzed experimental data.

REFERENCES

Ahmadlou, M., Houba, J.H.W., van Vierbergen, J.F.M., Giannouli, M., Gimenez, G.A., van Weeghel, C., Darbanfouladi, M., Shirazi, M.Y., Dziubek, J., Kacem, M., et al. (2021). A cell type-specific cortico-subcortical brain circuit for investigatory and novelty-seeking behavior. Science 372, eabe9681. https://doi.org/10.1126/science.abe9681.

Anderson, D.J., and Adolphs, R. (2014). A framework for studying emotions across species. Cell 157, 187–200. https://doi.org/10.1016/j.cell.2014.03.003.

Anthony, T.E., Dee, N., Bernard, A., Lerchner, W., Heintz, N., and Anderson, D.J. (2014). Control of stress-linduced persistent anxiety by an extra-amygdala septohypothalamic circuit. Cell 156, 522–536. https://doi.org/10.1016/j.cell.2013.12.040.

Barter, J.W., Li, S., Sukharnikova, T., Rossi, M.A., Bartholomew, R.A., and Yin, H.H. (2015). Basal ganglia outputs map instantaneous position coordinates during behavior. J. Neurosci. 35, 2703–2716. https://doi.org/10.1523/JNEUROSCI.3245-14.2015.

Bender, F., Gorbati, M., Cadavieco, M.C., Denisova, N., Gao, X., Holman, C., Korotkova, T., and Ponomarenko, A. (2015). Theta oscillations regulate the speed of locomotion via a hippocampus to lateral septum pathway. Nat. Commun. 6, 8521. https://doi.org/10.1038/ncomms9521.

Berger, S., Wolfer, D.P., Selbach, O., Alter, H., Erdmann, G., Reichardt, H.M., Chepkova, A.N., Welzl, H., Haas, H.L., Lipp, H.P., and Schütz, G. (2006). Loss of the limbic mineralocorticoid receptor impairs behavioral plasticity. Proc. Natl. Acad. Sci. USA 103, 195–200. https://doi.org/10.1073/pnas.0503878102.

Berlyne, D.E. (1966). Curiosity and exploration. Science 153, 25–33. https://doi.org/10.1126/science.153.3731.25.

Besnard, A., Gao, Y., TaeWoo Kim, M., Twarkowski, H., Reed, A.K., Langberg, T., Feng, W., Xu, X., Saur, D., Zweifel, L.S., et al. (2019). Dorsolateral septum somatostatin interneurons gate mobility to calibrate context-specific behavioral fear responses. Nat. Neurosci. 22, 436–446. https://doi.org/10.1038/s41593-018-0330-y.

Besnard, A., Miller, S.M., and Sahay, A. (2020). Distinct dorsal and ventral hippocampal CA3 outputs Govern contextual fear Discrimination. Cell Rep. 30, 2360–2373.e5, e2365. https://doi.org/10.1016/j.celrep.2020.01.055.

Cardin, J.A., Carlén, M., Meletis, K., Knoblich, U., Zhang, F., Deisseroth, K., Tsai, L.H., and Moore, C.I. (2010). Targeted optogenetic stimulation and recording of neurons in vivo using cell-type-specific expression of Channelrhodopsin-2. Nat. Protoc. 5, 247–254. https://doi.org/10.1038/nprot.2009.228.

Carus-Cadavieco, M., Gorbati, M., Ye, L., Bender, F., van der Veldt, S., Kosse, C., Börgers, C., Lee, S.Y., Ramakrishnan, C., Hu, Y., et al. (2017). Gamma oscillations organize top-down signalling to hypothalamus and enable food seeking. Nature 542, 232–236. https://doi.org/10.1038/nature21066.

Cezario, A.F., Ribeiro-Barbosa, E.R., Baldo, M.V.C., and Canteras, N.S. (2008). Hypothalamic sites responding to predator threats–the role of the dorsal premammillary nucleus in unconditioned and conditioned antipredatory defensive behavior. Eur. J. Neurosci. 28, 1003–1015. https://doi.org/10.1111/j.1460-9568.2008.06392.x.

Darwin, C. (1969). The Expression of the Emotions in Man and Animals (Greenwood Press).

De La Flor, M., Chen, L., Manson-Bishop, C., Chu, T.C., Zamora, K., Robbins, D., Gunaratne, G., and Roman, G. (2017). Drosophila increase exploration after visually detecting predators. PLoS One 12, e0180749. https://doi.org/10.1371/journal.pone.0180749.

Deacon, R.M.J. (2006). Digging and marble burying in mice: simple methods for in vivo identification of biological impacts. Nat. Protoc. 1, 122–124. https://doi.org/10.1038/nprot.2006.20.

Dudchenko, P.A., and Wallace, D. (2018). Neuroethology of spatial cognition. Curr. Biol. 28, R988–R992. https://doi.org/10.1016/j.cub.2018.04.051.

Esteban Masferrer, M., Silva, B.A., Nomoto, K., Lima, S.Q., and Gross, C.T. (2020). Differential encoding of predator fear in the ventromedial hypothalamus and periaqueductal grey. J. Neurosci. 40, 9283–9292. https://doi.org/10.1523/JNEUROSCI.0761-18.2020.

Evans, D.A., Stempel, A.V., Vale, R., and Branco, T. (2019). Cognitive control of escape behaviour. Trends Cogn. Sci. 23, 334–348. https://doi.org/10.1016/j.tics.2019.01.012.

Fanselow, M.S., and Dong, H.W. (2010). Are the dorsal and ventral Hippocampus functionally Distinct structures? Neuron 65, 7–19. https://doi.org/10.1016/j.neuron.2009.11.031.

Glaudas, X., Winne, C.T., and Fedewa, L.A. (2006). Ontogeny of anti-predator behavioral habituation in cottonmouths (Agkistrodon piscivorus). Ethology 112, 608–615. https://doi.org/10.1111/j.1439-0310.2005.01183.x.

Gottlieb, J., and Oudeyer, P.Y. (2018). Towards a neuroscience of active sampling and curiosity. Nat. Rev. Neurosci. 19, 758–770. https://doi.org/10.1038/s41583-018-0078-0.

Gottlieb, J., Oudeyer, P.Y., Lopes, M., and Baranes, A. (2013). Information-seeking, curiosity, and attention: computational and neural mechanisms. Trends Cogn. Sci. 17, 585–593. https://doi.org/10.1016/j.tics.2013.09.001.

Grailhe, R., Waeber, C., Dulawa, S.C., Hornung, J.P., Zhuang, X., Brunner, D., Geyer, M.A., and Hen, R. (1999). Increased exploratory activity and altered response to LSD in mice lacking the 5-HT(5A) receptor. Neuron 22, 581–591. https://doi.org/10.1016/s0896-6273(00)80712-6.

Gross, C.T., and Canteras, N.S. (2012). The many paths to fear. Nat. Rev. Neurosci. 13, 651–658. https://doi.org/10.1038/nrn3301.

Hanchate, N.K., Kondoh, K., Lu, Z., Kuang, D., Ye, X., Qiu, X., Pachter, L., Trapnell, C., and Buck, L.B. (2015). Single-cell transcriptomics reveals receptor transformations during olfactory neurogenesis. Science 350, 1251–1255. https://doi.org/10.1126/science.aad2456.

Headley, D.B., Kanta, V., Kyriazi, P., and Paré, D. (2019). Embracing complexity in defensive networks. Neuron 103, 189–201. https://doi.org/10.1016/j.neuron.2019.05.024.

Inoue, I., Yanai, K., Kitamura, D., Taniuchi, I., Kobayashi, T., Niimura, K., Watanabe, T., and Watanabe, T. (1996). Impaired locomotor activity and exploratory behavior in mice lacking histamine H1 receptors. Proc. Natl. Acad. Sci. USA 93, 13316–13320. https://doi.org/10.1073/pnas.93.23.13316.

Johnson, P.L., Truitt, W., Fitz, S.D., Minick, P.E., Dietrich, A., Sanghani, S., Träskman-Bendz, L., Goddard, A.W., Brundin, L., and Shekhar, A. (2010). A key role for orexin in panic anxiety. Nat. Med. 16, 111–115. https://doi.org/10.1038/nm.2075.

Kataoka, N., Shima, Y., Nakajima, K., and Nakamura, K. (2020). A central master driver of psychosocial stress responses in the rat. Science 367, 1105–1112. https://doi.org/10.1126/science.aaz4639.

Kim, E.J., Park, M., Kong, M.S., Park, S.G., Cho, J., and Kim, J.J. (2015). Alterations of hippocampal place cells in foraging rats facing a "predatory" threat. Curr. Biol. 25, 1362–1367. https://doi.org/10.1016/j.cub.2015.03.048.

Kitamura, T., Ogawa, S.K., Roy, D.S., Okuyama, T., Morrissey, M.D., Smith, L.M., Redondo, R.L., and Tonegawa, S. (2017). Engrams and circuits crucial for systems consolidation of a memory. Science 356, 73–78. https://doi.org/10.1126/science.aam6808.

Kondoh, K., Lu, Z., Ye, X., Olson, D.P., Lowell, B.B., and Buck, L.B. (2016). A specific area of olfactory cortex involved in stress hormone responses to predator odours. Nature 532, 103–106. https://doi.org/10.1038/nature17156.

Kunwar, P.S., Zelikowsky, M., Remedios, R., Cai, H., Yilmaz, M., Meister, M., and Anderson, D.J. (2015). Ventromedial hypothalamic neurons control a defensive emotion state. Elife 4, e06633. https://doi.org/10.7554/eLife.06633.

LeDoux, J. (2012). Rethinking the emotional brain. Neuron 73, 653–676. https://doi.org/10.1016/j.neuron.2012.02.004.

LeDoux, J., and Daw, N.D. (2018). Surviving threats: neural circuit and computational implications of a new taxonomy of defensive behaviour. Nat. Rev. Neurosci. 19, 269–282. https://doi.org/10.1038/nrn.2018.22.

Leroy, F., Park, J., Asok, A., Brann, D.H., Meira, T., Boyle, L.M., Buss, E.W., Kandel, E.R., and Siegelbaum, S.A. (2018). A circuit from hippocampal CA2 to lateral septum disinhibits social aggression. Nature 564, 213–218. https://doi.org/10.1038/s41586-018-0772-0.

Letzkus, J.J., Wolff, S.B.E., and Lüthi, A. (2015). Disinhibition, a circuit mechanism for associative learning and memory. Neuron 88, 264–276. https://doi.org/10.1016/j.neuron.2015.09.024.

Li, Y., Gao, X.B., Sakurai, T., and van den Pol, A.N. (2002). Hypocretin/Orexin excites hypocretin neurons via a local glutamate neuron-A potential mechanism for orchestrating the hypothalamic arousal system. Neuron 36, 1169–1181. https://doi.org/10.1016/s0896-6273(02)01132-7.

Lu, Y., Zhong, C., Wang, L., Wei, P., He, W., Huang, K., Zhang, Y., Zhan, Y., Feng, G., and Wang, L. (2016). Optogenetic dissection of ictal propagation in the hippocampal-entorhinal cortex structures. Nat. Commun. 7, 10962. https://doi.org/10.1038/ncomms10962.

Luo, A.H., Tahsili-Fahadan, P., Wise, R.A., Lupica, C.R., and Aston-Jones, G. (2011). Linking context with reward: a functional circuit from hippocampal CA3 to ventral tegmental area. Science 333, 353–357. https://doi.org/10.1126/science.1204622.

Markram, H., Toledo-Rodriguez, M., Wang, Y., Gupta, A., Silberberg, G., and Wu, C. (2004). Interneurons of the neocortical inhibitory system. Nat. Neurosci. 5, 793–807. https://doi.org/10.1038/nrn1519.

Martinez, R.C.R., Carvalho-Netto, E.F., Amaral, V.C.S., Nunes-de-Souza, R.L., and Canteras, N.S. (2008). Investigation of the hypothalamic defensive system in the mouse. Behav. Brain Res. 192, 185–190. https://doi.org/10.1016/j.bbr.2008.03.042.

Mobbs, D. (2018). The ethological deconstruction of fear(s). Curr. Opin. Behav. Sci. 24, 32–37. https://doi.org/10.1016/j.cobeha.2018.02.008.

Mobbs, D., Trimmer, P.C., Blumstein, D.T., and Dayan, P. (2018). Foraging for foundations in decision neuroscience: insights from ethology. Nat. Rev. Neurosci. 19, 419–427. https://doi.org/10.1038/s41583-018-0010-7.

Naka, A., and Adesnik, H. (2016). Inhibitory circuits in cortical layer 5. Front. Neural Circuits 10, 35. https://doi.org/10.3389/fncir.2016.00035.

Padilla, S.L., Qiu, J., Soden, M.E., Sanz, E., Nestor, C.C., Barker, F.D., Quintana, A., Zweifel, L.S., Rønnekleiv, O.K., Kelly, M.J., and Palmiter, R.D. (2016). Agouti-related peptide neural circuits mediate adaptive behaviors in the starved state. Nat. Neurosci. 19, 734–741. https://doi.org/10.1038/nn.4274.

Pérez-Gómez, A., Bleymehl, K., Stein, B., Pyrski, M., Birnbaumer, L., Munger, S.D., Leinders-Zufall, T., Zufall, F., and Chamero, P. (2015). Innate predator odor aversion driven by parallel olfactory subsystems that converge in the ventromedial hypothalamus. Curr. Biol. 25, 1340–1346. https://doi.org/10.1016/j.cub.2015.03.026.

Piñol, R.A., Zahler, S.H., Li, C., Saha, A., Tan, B.K., Škop, V., Gavrilova, O., Xiao, C., Krashes, M.J., and Reitman, M.L. (2018). Brs3 neurons in the mouse dorsomedial hypothalamus regulate body temperature, energy expenditure, and heart rate, but not food intake. Nat. Neurosci. 21, 1530–1540. https://doi.org/10.1038/s41593-018-0249-3.

Qi, S., Hassabis, D., Sun, J., Guo, F., Daw, N., and Mobbs, D. (2018). How cognitive and reactive fear circuits optimize escape decisions in humans. Proc. Natl. Acad. Sci. USA 115, 3186–3191. https://doi.org/10.1073/pnas.1712314115.

Ribeiro-Barbosa, E.R., Canteras, N.S., Cezário, A.F., Blanchard, R.J., and Blanchard, D.C. (2005). An alternative experimental procedure for studying predator-related defensive responses. Neurosci. Biobehav. Rev. *29*, 1255–1263. https://doi.org/10.1016/j.neubiorev.2005.04.006.

Risold, P.Y., and Swanson, L.W. (1996). Structural evidence for functional domains in the rat hippocampus. Science *272*, 1484–1486. https://doi.org/10.1126/science.272.5267.1484.

Saab, B.J., Georgiou, J., Nath, A., Lee, F.J.S., Wang, M., Michalon, A., Liu, F., Mansuy, I.M., and Roder, J.C. (2009). NCS-1 in the dentate gyrus promotes exploration, synaptic plasticity, and rapid acquisition of spatial memory. Neuron *63*, 643–656. https://doi.org/10.1016/j.neuron.2009.08.014.

Sano, Y., Ornthanalai, V.G., Yamada, K., Homma, C., Suzuki, H., Suzuki, T., Murphy, N.P., and Itohara, S. (2009). X11-like protein deficiency is associated with impaired conflict resolution in mice. J. Neurosci. *29*, 5884–5896. https://doi.org/10.1523/JNEUROSCI.5756-08.2009.

Siemian, J.N., Sarsfield, S., and Aponte, Y. (2020). Glutamatergic fast-spiking parvalbumin neurons in the lateral hypothalamus: electrophysiological properties to behavior. Physiol. Behav. *221*, 112912. https://doi.org/10.1016/j.physbeh.2020.112912.

Silva, B.A., Mattucci, C., Krzywkowski, P., Murana, E., Illarionova, A., Grinevich, V., Canteras, N.S., Ragozzino, D., and Gross, C.T. (2013). Independent hypothalamic circuits for social and predator fear. Nat. Neurosci. *16*, 1731–1733. https://doi.org/10.1038/nn.3573.

Strange, B.A., Witter, M.P., Lein, E.S., and Moser, E.I. (2014). Functional organization of the hippocampal longitudinal axis. Nat. Rev. Neurosci. *15*, 655–669. https://doi.org/10.1038/nrn3785.

Sturman, O., Germain, P.L., and Bohacek, J. (2018). Exploratory rearing: a context- and stress-sensitive behavior recorded in the open-field test. Stress *21*, 443–452. https://doi.org/10.1080/10253890.2018.1438405.

Sweeney, P., and Yang, Y. (2015). An excitatory ventral hippocampus to lateral septum circuit that suppresses feeding. Nat. Commun. *6*, 10188. https://doi.org/10.1038/ncomms10188.

Sweeney, P., and Yang, Y. (2016). An inhibitory septum to lateral hypothalamus circuit that suppresses feeding. J. Neurosci. *36*, 11185–11195. https://doi.org/10.1523/JNEUROSCI.2042-16.2016.

Tingley, D., and Buzsáki, G. (2018). Transformation of a spatial map across the hippocampal-lateral septal circuit. Neuron *98*, 1229–1242.e5. https://doi.org/10.1016/j.neuron.2018.04.028.

Tovote, P., Fadok, J.P., and Lüthi, A. (2015). Neuronal circuits for fear and anxiety. Nat. Rev. Neurosci. *16*, 317–331. https://doi.org/10.1038/nrn3945.

Trenk, A., Walczak, M., Szlaga, A., Pradel, K., Blasiak, A., and Blasiak, T. (2022). Bidirectional communication between the pontine nucleus incertus and the medial septum is carried out by electrophysiologically-Distinct

neuronal populations. J. Neurosci. *42*, 2234–2252. https://doi.org/10.1523/JNEUROSCI.0230-21.2022.

Ucar, H., Watanabe, S., Noguchi, J., Morimoto, Y., Iino, Y., Yagishita, S., Takahashi, N., and Kasai, H. (2021). Mechanical actions of dendritic-spine enlargement on presynaptic exocytosis. Nature *600*, 686–689. https://doi.org/10.1038/s41586-021-04125-7.

van Kampen, H.S. (2015). Violated expectancies: cause and function of exploration, fear, and aggression. Behav. Processes *117*, 12–28. https://doi.org/10.1016/j.beproc.2014.05.005.

Vander Weele, C.M., Siciliano, C.A., Matthews, G.A., Namburi, P., Izadmehr, E.M., Espinel, I.C., Nieh, E.H., Schut, E.H.S., Padilla-Coreano, N., Burgos-Robles, A., et al. (2018). Dopamine enhances signal-to-noise ratio in cortical-brainstem encoding of aversive stimuli. Nature *563*, 397–401. https://doi.org/10.1038/s41586-018-0682-1.

Wang, C.A., Baird, T., Huang, J., Coutinho, J.D., Brien, D.C., and Munoz, D.P. (2018). Arousal effects on pupil size, heart rate, and skin conductance in an emotional face task. Front. Neurol. *9*, 1029. https://doi.org/10.3389/fneur.2018.01029.

Wang, X., Liu, H., Morstein, J., Novak, A.J.E., Trauner, D., Xiong, Q., Yu, Y., and Ge, S. (2020). Metabolic tuning of inhibition regulates hippocampal neurogenesis in the adult brain. Proc. Natl. Acad. Sci. USA *117*, 25818–25829. https://doi.org/10.1073/pnas.2006138117.

Wascher, C.A.F. (2021). Heart rate as a measure of emotional arousal in evolutionary biology. Philos. Trans. R. Soc. Lond. B Biol. Sci. *376*, 20200479. https://doi.org/10.1098/rstb.2020.0479.

Wei, P., Liu, N., Zhang, Z., Liu, X., Tang, Y., He, X., Wu, B., Zhou, Z., Liu, Y., Li, J., et al. (2015). Processing of visually evoked innate fear by a non-canonical thalamic pathway. Nat. Commun. *6*, 6756. https://doi.org/10.1038/ncomms7756.

Wikenheiser, A.M., and Schoenbaum, G. (2016). Over the river, through the woods: cognitive maps in the hippocampus and orbitofrontal cortex. Nat. Rev. Neurosci. *17*, 513–523. https://doi.org/10.1038/nrn.2016.56.

Wong, L.C., Wang, L., D'Amour, J.A., Yumita, T., Chen, G., Yamaguchi, T., Chang, B.C., Bernstein, H., You, X., Feng, J.E., et al. (2016). Effective modulation of male aggression through lateral septum to medial hypothalamus projection. Curr. Biol. *26*, 593–604. https://doi.org/10.1016/j.cub.2015.12.065.

Zelikowsky, M., Hui, M., Karigo, T., Choe, A., Yang, B., Blanco, M.R., Beadle, K., Gradinaru, V., Deverman, B.E., and Anderson, D.J. (2018). The neuropeptide Tac2 controls a distributed brain state induced by chronic social isolation stress. Cell *173*, 1265–1279.e19. https://doi.org/10.1016/j.cell.2018.03.037.

Zhu, J., Ji, L., and Liu, C. (2019). Heart rate variability monitoring for emotion and disorders of emotion. Physiol. Meas. *40*, 064004. https://doi.org/10.1088/1361-6579/ab1887.

Cell Reports
Article

STAR★METHODS

KEY RESOURCES TABLE

REAGENT or RESOURCE	SOURCE	IDENTIFIER
Antibodies		
Anti-DIG-POD antibodies	Roche	Cat#1207733910
C-Fos	Cell Signal Technology	Cat#2250
Alexa Fluor 488-conjugated AffiniPure goat anti-rabbit IgG	Jackson ImmunoResearch	Cat#111-547-003
Alexa Fluor 594-conjugated AffiniPure goat anti-rabbit IgG	Jackson ImmunoResearch	Cat#111-585-003
Bacterial and virus strains		
AAV2/9-Ef1α-DIO-His-EGFP-2a-TVA-WPRE-pA	BrainVTA	PT-0023
AAV2/9-Ef1α-DIO-RVG-WPRE-pA	BrainVTA	PT-0021
RV-EvnA-ΔG-dsRed	BrainVTA	R01002
AAV9-CaMKIIα-ChR2-mCherry	BrainVTA	PT-0297
AAV9-Ef1α-DIO-ChR2-mCherry	BrainVTA	PT-0002
AAV9-CaMKII-eArchT-EYFP	WZ Biosciences	N/A
AAV9-Ef1α-DIO-eArch3.0-EYFP	WZ Biosciences	N/A
AAV9-CaMKIIα-mCherry	This paper	N/A
AAV9-Ef1α-DIO-mCherry	This paper	N/A
Chemicals, peptides, and recombinant proteins		
CTB-594	Molecular Probes	C-34777
DAPI	Beyotime	c1002
Proteinase K	Roche	03115828001
DEPC	Sigma	D5758
EDTA	Thermo Fisher	AM9261
20× standard saline citrate [SSC]	Thermo Fisher	AM9765
50× Denhardt solution	Sigma	D2532
blocking reagent	Perkin Elmer	FP1020
TSA plus Cy3 kit	Perkin Elmer	NEL744001KT
Fluoromount-G	Southern Biotech	0100-01
Normal goat serum	Jackson Immuno Research	005-000-121
Experimental models: Organisms/strains		
Mouse: C57BL/6J	Guangdong Medical Laboratory Animal Center, China	N/A
Mouse: GAD2-IRES-Cre	The Jackson Laboratory	JAX stock # 010802
Mouse: VGAT-ChR2(H134R)-EYFP	The Jackson Laboratory	JAX stock # 014548
Rat: Sprague-Dawley (SD)	Guangdong Medical Laboratory Animal Center, China	N/A
Software and algorithms		
Plexon Offline Sorter software	Plexon	https://plexon.com/products/offline-sorter/
MATLAB	MathWorks	https://ww2.mathworks.cn
Neuroexplorer	Plexon	https://plexon.com/products/neuroexplorer/
MATLAB script for spike analysis	This paper	Zenodo: http://doi.org/10.5281/zenodo.7115045
Other		
Optical fibers	Thorlabs	N/A
Formvar-coated nickel chromium wires	California Fine Wire Company	N/A

RESOURCE AVAILABILITY

Lead contact
Further information and requests for resources and reagents should be directed to and will be fulfilled by the lead contact, Liping Wang (lp.wang@siat.ac.cn).

Materials availability
All materials developed in this study will be available from the lead contact upon request.

Data and code availability
- All data reported in this study will be available from the lead contact upon request.
- All original code has been deposited at Zenodo and is publicly available as of the date of publication. DOIs are listed in the key resources table.
- Any additional information required to reanalyze the data reported in this paper is available from the lead contact upon request.

EXPERIMENTAL MODEL AND SUBJECT DETAILS

Animals
All animal experiments were performed in accordance with the protocols approved by the Ethics Committee for Animal Research, Shenzhen Institute of Advanced Technology, Chinese Academy of Sciences. Groups of six- to eight-week-old male C57BL/6J wild-type mice (Guangdong Medical Laboratory Animal Center, China), GAD2-IRES-Cre transgenic mice (Jackson Laboratory, repository number: 010802) and eight- to 10-week-old male VGAT-ChR2(H134R)-EYFP transgenic mice were used in our study. Groups of eight- to 12-week-old male Sprague-Dawley (SD) wild-type rats (Guangdong Medical Laboratory Animal Center, China) were employed as predators. Animals were housed under controlled conditions (ambient temperature 24 ± 1 °C, humidity 50%–60%, lights on from 08:00 to 20:00) with food and water *ad libitum*.

METHOD DETAILS

Virus injections
Isoflurane (Attane, induction 3%, maintenance 1.5%; Provet) in oxygen-enriched air was used to anesthetize mice fixed in a stereotactic frame (Kopf Instruments 1900 series). A 33-gauge metal needle connected to a microsyringe pump (UMP3/Micro4) was used to infuse the viruses at a rate of 100 nL/min. After infusion, the needle was kept at the injection site for 10 min and then slowly withdrawn before the incision was sutured.

To determine the inputs to the dLS and DMH, respectively, 0.15 μL of CTB-594 (C-34777, Molecular Probes) was injected into the dLS (AP +0.74 mm, ML -0.30 mm, DV -3.00 mm) or DMH (AP -1.60 mm, ML -0.40 mm, DV -4.85 mm). Mice were housed for 7 days to allow the expression of fluorescent proteins in presynaptic cells.

To determine whether dLS serves as a relay for the dHPC-DMH circuit, 0.3 μL of AAV2/9-Ef1α-DIO-His-EGFP-2a-TVA-WPRE-pA and AAV2/9-Ef1α-DIO-RVG-WPRE-pA mixture (PT-0021, 2×10^{12} vg/ml, BrainVTA) was injected into the dLS of GAD-Cre transgenic mice. We injected G-deleted rabies virus (RV-ΔG, RV-EvnA-ΔG-dsRed, R01002, 2×10^{8} IFU/mL, BrainVTA) into the DMH after the expression of AAV-helper in the dLS of GAD-cre transgenic mice. For the no G protein control experiment, 0.3 μl of AAV2/9-Ef1α-DIO-His-EGFP-2a-TVA-WPRE-pA (PT-0023, 2×10^{12} vg/ml, BrainVTA) was injected into the dLS of GAD2-IRES-Cre transgenic mice. 3–4 weeks after that, 0.1 μl of RV-ENVA-ΔG-dsRed (R01002, 2×10^{8} vg/ml, BrainVTA) was injected into the DMH. Mice were then housed for 12 days to allow the viral expression in the target cells. The entire brain was sectioned and imaged using a slide scanner (VS120, Olympus).

For optogenetic activation of the dHPC^{Glu} neurons and the dHPC^{Glu}–dLS projections, 0.3 μL of AAV9-CaMKIIα-ChR2-mCherry (PT-0297, 2×10^{12} vg/ml, BrainVTA) was injected into the dCA3 (AP -2.06 mm, ML -1.80 mm, DV -1.85 mm) of C57BL/6J wild-type mice. For optogenetic excitation of dLS^{GABA} neurons or dLS^{GABA}–DMH projections, 0.3 μL of AAV9-Ef1α-DIO-ChR2-mCherry (PT-0002, 2×10^{12} vg/ml, BrainVTA) was injected into the dLS of GAD2-IRES-Cre transgenic mice. For optogenetic inhibition of the dHPC^{Glu}–dLS projections, 0.3 μL of AAV9-CaMKII-eArchT-EYFP (4×10^{12} vg/ml, WZ Biosciences) was injected into the dCA3 of C57BL/6J wild-type mice. For optogenetic inhibition of dLS^{GABA}–DMH projections, 0.3 μL of AAV9-Ef1α-DIO-eArch3.0-EYFP (4×10^{12} vg/ml, WZ Biosciences) was injected into the dLS of GAD2-IRES-Cre transgenic mice. For control experiment of optogenetic stimulation of dHPC^{Glu} neurons and dHPC^{Glu}–dLS projections, 0.3 μL of AAV9-CaMKIIα-mCherry (2×10^{12} vg/ml, Liping Wang's Lab at the SIAT CAS) was injected into the dCA3 of C57BL/6J wild-type mice. For control experiment of optogenetic stimulation of dLS^{GABA}–DMH projections, 0.3 μL of AAV9-Ef1α-DIO-mCherry (2×10^{12} vg/ml, Liping Wang's Lab at the SIAT CAS) was injected into the dLS of GAD2-IRES-Cre transgenic mice. The animals were allowed to recover, and their viral expression was monitored for 4 weeks.

Fabrication of implants

Optical implants were fabricated from optical fibers (0.37 numerical aperture [NA], Thorlabs) and optical ceramic ferrules. For optogenetic stimulation and electrophysiological recordings in anesthetized mice, acute multi-channel optrode arrays, each containing one optical channel and eight twisted stereotrodes (16 channels in total), were fabricated from optical fibers (200 μm diameter, 0.37 NA, Thorlabs) and formvar-coated nickel chromium wires (17-μm diameter, California Fine Wire Company). Each stereotrode was threaded through a silica tube (75-μm inner and 150-μm outer diameters, Polymicro Technologies) and arranged around an optical fiber using a custom-made optrode mold. To ensure illumination of the recorded neurons in each optrode array, the electrical recording sites were $\sim$ 400 μm deeper than the optical fiber. The electrochemical impedance of each recording site was decreased to $\sim$ 500 kΩ (at 1 kHz in artificial cerebrospinal fluid [ACSF]) prior to use. Two pairs of silver microwires (100-μm diameter) were soldered onto the electrode connector as the ground and reference electrodes, respectively.

For electrophysiological recordings in free-moving mice in PTT, drivable microwire electrode arrays were fabricated from formvar-coated nickel chromium wires (17-μm diameter, California Fine Wire Company). Each stereotrode was also threaded through a silica tube (75-μm inner diameter and 150-μm outer diameter, Polymicro Technologies), and 10 stereotrodes in silica tubes were arranged in a custom-made drivable three-layer nested structure. Finally, a drivable microwire electrode array with a nested structure was obtained, and platinum nanoparticles were deposited on the tip of the microwires to decrease their impedance to $\sim$500 kΩ (at 1 kHz in ACSF) prior to use.

Implantation surgery and optogenetics

The mice were implanted with optical implants for optogenetic manipulation *in vivo*. For optical activation of the dCA3^{Glu} or dCA3^{VGAT} neurons, the tip of optical fiber was lowered into the dCA3 (AP -2.06 mm, ML -1.80 mm, DV -1.65 mm). For optical stimulation of the dLS^{GABA} neurons or dCA3^{Glu}-dLS circuit, the tip of the optical fiber was lowered into the dLS (AP +0.74 mm, ML -0.30 mm, DV -2.75 mm). For optical manipulations of the dLS^{GABA}-DMH circuit, the tip of the optical fiber was lowered into the DMH (AP -1.60 mm, ML -0.40 mm, DV -4.65 mm). All optical fibers were tested for effective light transduction before the implantation. The animals were allowed to recover for at least 1 week after surgery.

For electrophysiological recording from the dCA3-dLS-DMH circuit in PTT, drivable microwire electrode arrays were implanted into the dCA3 (AP -2.06 mm, ML -1.80 mm, DV -2.25 mm), dLS (AP +0.74 mm, ML -0.30 mm, DV -3.10 mm), or DMH (AP -1.60 mm, ML -0.40 mm, DV -5.00 mm). The implants were fixed to the skull using skull screws and dental cement. The animals were allowed to recover for 7–10 days after the surgery before testing.

Predator threat test (PTT) and behavioral analysis

Following previous studies (De La Flor et al., 2017; Kim et al., 2015; Ribeiro-Barbosa et al., 2005; Silva et al., 2013), the behavior of mice was tested using the PTT. The PTT apparatus was composed of similar detachable home and test chambers (HC and TC, 25 cm × 25 cm × 25 cm) that were connected via a narrow corridor (NC, 12.5-cm wide, 60-cm long, 30-cm high) terminated by a door (2.5-cm wide) at each end. Both doors could be opened and closed manually, and only the mice (not the predatory rat) could pass through. The experimental paradigm is depicted in Figure S1A. Each mouse subject was housed in the HC for 2 h on three consecutive days for habituation (days 1–3, habituation I) and was then allowed to access the entire apparatus for 20 min per day for another three days (days 4–6, habituation II). On day 7, the PTT was performed in two steps: First, the experimental subject was free to explore the entire apparatus for 10 min (No Rat period). Then, this mouse was confined to the TC by closing the door, and a predatory rat was placed in the TC. The mouse was kept with the rat for 5 s, allowing interactions to occur before the door was re-opened to allow it to escape. The behaviors of the mice were monitored in the presence of the predatory rat (confined to the TC) for a further 10 min (rat test). Defensive behaviors were scored during the No Rat and Rat periods. Before testing each subject, the apparatus was cleaned with a 50% ethanol aqueous solution (vol/vol).

To investigate light-mediated effects on the behaviors of the mice during the Rat period, the mice were allowed to move freely within the apparatus for 30 min in the presence of a predatory rat: 10 min before, 10 min during optogenetic stimulation, respectively. For optogenetic activation, laser light pulses (473 nm, 5-ms pulse duration) controlled by an analog input were used (Cardin et al., 2010; Ucar et al., 2021; Vander Weele et al., 2018). The light density was adjusted with an optical power meter (Thorlabs) to reach 10 mW and 15 mW for the activation of the somas and terminals, respectively. Light pulses with frequencies of 11 Hz, 20 Hz, and 40 Hz were used to activate dCA3^{VGAT}, dCA3^{Glu}, and dLS^{GABA} neurons, respectively. For optogenetic inhibition, a constant yellow light was delivered (589 nm) through dual-core fiber patch cables with 20 mW at fiber tip.

The behaviors of the test subjects were monitored using a custom-made dual-camera system and tracked offline using the software package AnyMaze (Stoelting). Defensive behavior-related parameters, including the time spent in the HC (safe zone), and entries into the NC were calculated. During the Rat period, detailed behavioral assessments were performed using the behavioral checklist method (Deacon, 2006; Grailhe et al., 1999; Inoue et al., 1996; Sano et al., 2009). To evaluate the exploratory activity of the mice, the behaviors in each test period were counted, including digging, rearing, and exploring at the HC door (head direction: HC-NC) and the TC door (head direction: NC-TC). Neutral exploration was defined as the animal exploring the safe zone, including all digging and rearing in the HC. Risk exploration was defined as the animal exploring the dangerous zone, including rearing in the NC and exploring at the HC door. High-risk exploration was defined as the animal exploring at the TC door. The total exploratory activity was defined as the sum of neutral, risk, and high-risk exploratory activities.

Open field test (OFT)

Mice were placed in the center of an open square arena (length: width: height, 50: 50: 60 cm) and videotaped individually. To assess the effect of optogenetic stimulation of dCA3-dLS-DMH circuitry on locomotor activity, mice were tested in 20-min sessions, consisting of 10-min light off and 10-min light on periods. The distance traveled in the OFT were automatically analyzed by ANY-maze.

Electrophysiological recordings

Electrophysiological recordings in anesthetized mice were performed following procedures reported in previous studies (Lu et al., 2016; Wei et al., 2015). Briefly, after the animal's head was fixed in a standard stereotaxic frame, the cranium was exposed through a small midline scalp incision. Holes were drilled through the skull, and optrode arrays were directed toward the targeted brain regions for optical stimulation and electrical recordings. Blue light pulses were delivered via the implanted optrode arrays with a cycling stimulation mode (30 s on, 150 s off).

To investigate the neural circuit processing mechanisms at the functional level, electrophysiological recordings in free-behaving mice were performed during the No Rat and Rat period, respectively. During the recording sessions, a preamplifier (Plexon) was connected to the output connector of each optrode array, and electrophysiological recordings were performed using a multichannel neural acquisition processor (Plexon). Single and multi-unit recordings were sampled at 40 kHz and bandpass-filtered at 300–5000 Hz.

Electrophysiological data analysis

Neural signal analyses were performed using Plexon Offline Sorter software (Plexon) and a custom-designed MATLAB (MathWorks) code. Individual spikes were detected by setting a threshold at five times the standard deviation (SD) and were measured within a 1400-μs time window. Principal component scores were calculated for the unsorted aligned waveforms and plotted on the three-dimensional (3D) principal component spaces. The cluster was clearly distinguished from the others in the 3D principal components plane using the L-ratio (< 0.2) and isolation distance (> 18). Units with an L-ratio > 0.2 and an isolation distance < 18 were excluded from the subsequent analysis. To characterize putative inhibitory neurons (PI) and putative excitatory neurons (PE), two features of the extracellular waveform, the peak-to-peak time and the half-width of the spikes, were calculated. Neurons with narrow and wide peaks were regarded as PI and PE, respectively. In addition, we classified dLS and DMH neurons into two classes based on firing rate: class I, firing rate of average < 2 Hz; class II, firing rate of average > 2 Hz.

Peri-event raster plots and waveforms were created using Neuroexplorer software. For the peri-event raster plot, optogenetic stimulation-induced neural activity was calculated from 90-s segments of continuous neural recordings (from 30 s before to 30 s after optical stimulation) using counts/bin (bin = 10 s). Auto-correlogram histograms and z-score normalized firing rates were created using the MATLAB software. Z-score values were calculated by subtracting the average baseline firing rate over the 60 s period preceding stimulus onset and divided by the SD of the baseline.

In free-moving recordings, because of the average firing rates of recorded neurons are variable, proper normalization was used instead of firing rates to investigate the overall response of neuronal activity (Barter et al., 2015). To intuitively compare the changes of neuronal activity during a pair of behaviors transition, z-score normalized firing rates during the HC-NC transition, fleeing-after fleeing transition, were calculated by subtracting the average baseline (the firing rate 5 s before behavior event onset) and divided by the SD of the baseline across all trials, separately for each unit. To compare the changes in neuronal activity between different events in the behavioral test, the NFRD was calculated by subtracting the average firing rate of the entire period from that of a behavioral event and dividing the difference by the average firing rate of the entire period across all trials (in the HC, in the NC, exploration at the HC door, before entering the NC, exploration at the TC door, separately for each unit).

$$\text{NFRD} = \frac{FR - FR_{average}}{FR_{average}}$$

The distribution of NFRD was analyzed to quantify the response distribution of all neurons to a behavioral event (Figures 1 and 5). In addition, if the NFRD of a neuron was greater than 1, we calculated it as 1.05. In other words, all neurons with NFRD >1 were considered to have NFRD = 1.05.

Histology

After the experiments had been concluded, mice were deeply anesthetized and perfused through the ascending aorta with 0.1 M phosphate-buffered saline (PBS, pH 7.3) followed by 4% paraformaldehyde in 0.1 M PBS. The brains were removed quickly from the skull and incubated in 4% PFA at 4°C overnight for post-fixation. After thorough rinsing in 0.1 M PBS, the brains were cryoprotected in 0.1 M PBS containing 30% sucrose for 72 h. The brains were embedded in optimum cutting temperature compound, snap-frozen at −20°C, and stored at −80°C. Coronal sections with a thickness of 35 μm were prepared using a cryostat microtome (Leica, CM1950). The brain sections were washed in 0.1 M PBS for 10 min. After that, the sections were mounted onto gelatin-coated slides and coverslipped with fluoromount (ProLong Gold Antifade Reagent with DAPI, P36935, Invitrogen). The mounted slices were observed using an inverted confocal microscope (Zeiss, LSM880 with Airyscan).

Immunohistochemistry for c-Fos protein

All groups of animals were sacrificed and perfused 90 min after PTT, following the paradigm Figure S1B. Another group of mice, which was housed in a home cage, was sacrificed and perfused as a control group. The detailed experimental design is summarized in Figure S1B. *In situ* hybridization (ISH) was performed as previously described (Hanchate et al., 2015; Kondoh et al., 2016). For RNA ISH, 25-μm thick brain sections were obtained using a cryostat microtome (Leica, CM1950). The sections were mounted individually on SuperFrost Plus slides (Fisher Scientific) for ISH (6 slices/slide). Slides were dried at 65°C for 5 min, incubated at room temperature (RT) in 0.02% Triton-X 100 DEPC PBS (1:1000 DEPC diluted 1 × PBS) for 3 min, and washed for 3 min in DEPC PBS. The slices were then incubated in 0.2% H_2O_2 DEPC PBS for 15 min and washed twice with DEPC PBS for 3 min. For high-sensitivity ISH, the slices were treated with Proteinase K (0.08 μg/mL, 03115828001, Roche; diluted in 1 M Tris PH 7.5, 0.5 M EDTA, DEPC PBS) for 10 min, washed for 3 min in 0.2% glycine DEPC PBS, incubated for 15 min in 0.25 acetic anhydride and 0.1 M triethanolamine buffer, followed by two washing steps, each for 3 min at room temperature in DEPC PBS. Next, the slices were hybridized with 1:200 RNA probes (GAD 1/2 or VGLUT 1/2 probe, 40 ng/μL) in hybridization buffer (50% formamide, 20× standard saline citrate [SSC], 50× Denhardt solution, yeast RNA, 1 M DTT, 0.1% volume of herring sperm DNA) at 56 °C overnight. The slices were then washed for 5 min in 2× SSC and 20 min in 0.2× SSC at 65 °C, followed by 20 min at RT in 0.2× SSC. The slices were incubated with Anti-DIG-POD antibodies (1:300, 1207733910, Roche) diluted in blocking buffer (0.1 M Tris-HCl pH 7.5, 0.15 M NaCl, 0.5% blocking reagent [FP1020, Perkin Elmer]) for 45 min at 37°C, and then washed three times for 5 min at RT in TNT (0.1 M Tris-HCl pH 7.5, 0.5 M NaCl, 0.05% Tween20) buffer. Next, the slices were incubated for 10 min in TSA-cy3 (1:100; NEL744001KT, TSA plus Cy3 kit; Perkin Elmer) followed twice for 5 min in TNT buffer.

For c-Fos staining, the slices were incubated with c-Fos primary antibodies (1:200, c-Fos [9F6] rabbit mAb, #2250, Cell Signal Technology) in PBS, supplemented with 5% BSA and 0.2% Triton-X 100, for 3 h at 37°C, and washed twice for 5 min in TNT buffer. The slices were then incubated with secondary antibodies (1:100, Alexa Fluor 488-conjugated AffiniPure goat anti-rabbit IgG, 111-547-003, Jackson ImmunoResearch) for 30 min at 37°C and washed twice for 5 min in TNT buffer. The slices were then incubated for 10 min in DAPI (1:2000, c1002, Beyotime) and washed twice for 5 min in TNT buffer. Slides were mounted with Fluoromount-G (0100-01; I1516-W896, Southern Biotech) and then evaluated for fluorescence using Alexa Fluor 488 (green), 543 (red), and 405 (blue) on an inverted confocal microscope (Zeiss, LSM880 with Airyscan).

To quantify the increased neuronal activity after PTT, the slices were treated with PBS three times for 10 min each and blocked in 10% normal goat serum (005-000-121, Jackson Immuno Research) for 1 h. The samples were then incubated with primary antibodies (1:200; c-Fos [9F6] rabbit mAb, #2250, Cell Signal Technology) overnight at 4°C and diluted with 3% NGS and 0.1% triton-x in PBS. Next, the slices were washed with PBS three times for 10 min each and incubated for 2 h with secondary antibodies (1:200, Alexa Fluor 594-conjugated AffiniPure goat anti-rabbit IgG, 111-585-003, Jackson Immuno Research). After washing with PBS three times for 10 min each, the slices were mounted onto gelatin-coated slides and cover slipped with mounting medium (VECTASHIELD Anti-fade Mounting Medium with DAPI, H-1200, Vector Laboratories, Inc.). Slices were evaluated for fluorescence using a virtual slide system (Olympus, VS120-S6-W).

Heart rate (HR) measurements

HR was recorded using a pulse oximeter (MouseOx Plus; Starr Life Sciences). For HR recording in an anesthetized mouse, hair was removed from the mouse's neck skin with depilation cream (VEET® Gel), and a sensor was attached to the neck of the mouse to obtain HR signals from the carotid arteries. To investigate light-mediated effects on the HR of the mice, a continuous HR baseline (300 s) was recorded before blue light pulses were conducted (30 s). Prior to HR measurements in freely behaving animals, the test subjects were habituated to the sensors for 10 min per day for 3 consecutive days. To study the relationship between HR and predatory threat, the HR of mice was tested in the HC and TC (occupied by a predatory rat). Optogenetic stimulation (180 s) was performed to investigate the influence of dCA3^{Glu}-dLS and dLS^{GABA}-DMH circuit activation on HR in the presence of a predator.

QUANTIFICATION AND STATISTICAL ANALYSIS

Data were analyzed using two-tailed, paired, or two-sample t-tests using the Origin software. All data are presented as mean ± standard deviation of the mean (mean ± SD). Significance levels are indicated as follows: *$p < 0.05$, **$p < 0.01$, and ***$p < 0.005$. The statistical details are shown in the respective figure legends.